DR. JOHN J BISSLER (Orcid ID : 0000-0001-9685-9183)

Article type : Original Article

Tuberous Sclerosis Complex Exhibits a New Renal Cystogenic Mechanism

Authors: John J. Bissler[1,2], Fahad Zadjali[3], Dave Bridges[4], Aristotelis Astrinidis[1,] Sharon Barone [5,6,7], Ying Yao[1], JeAnna R. Redd[4], Brian J. Siroky[8], Yanqing Wang[9], Joel T. Finley[1], Michael E. Rusiniak[9], Heinz Baumann[9], Kamyar Zahedi[,5,6,7], Kenneth W. Gross[9], Manoocher Soleimani[5,6,7]

Affiliations

[1]Department of Pediatrics, University of Tennessee Health Science Center and Le Bonheur Children's Hospital, Memphis, TN.

[2]St. Jude Children's Research Hospital, Memphis, TN.

[3]Department of Clinical Biochemistry , College of Medicine & Health Sciences, Sultan Qaboos University

[4]Department of Nutritional Sciences, University of Michigan School of Public Health, Ann Arbor, MI

[5]Departments of Medicine, University of Cincinnati College of Medicine, Cincinnati, OH, United States of America.

[6]Center on Genetics of Transport, University of Cincinnati College of Medicine, Cincinnati, OH, United States of America.

[7]Research Services, Veterans Affairs Medical Center, Cincinnati, OH, United States of America.

This is the author manuscript accepted for publication and has undergone full peer review but has not been through the copyediting, typesetting, pagination and proofreading process, which may lead to differences between this version and the Version of Record. Please cite this article as doi: 10.14814/phy2.13983

[8]Department of Pediatrics, University of Cincinnati College of Medicine, Cincinnati, OH, United States of America.

[9]Department of Molecular and Cellular Biology, Roswell Park Cancer Institute, Buffalo, NY

*To whom correspondence should be addressed:

John J. Bissler, MD
FedEx Chair of Excellence
Department of Pediatrics, UTHSC
51N. Dunlap St.
Memphis, TN 38103
jbissler@uthsc.edu

One Sentence Summary: Tuberous sclerosis complex (TSC) patients develop renal cysts by a novel induction mechanism.

Abstract. Tuberous sclerosis complex (TSC) is a tumor predisposition syndrome with significant renal cystic and solid tumor disease. While the most common renal tumor in TSC, the angiomyolipoma, exhibits a loss of heterozygosity associated with disease, we have discovered that the renal cystic epithelium is composed of type A intercalated cells that have an intact *Tsc* gene that have been induced to exhibit *Tsc*-mutant disease phenotype. Although this mechanism appears to be different than that for ADPKD, it still is mTORC1 inhibitor responsive. The murine models described here closely resemble the human disease and both appear to be mTORC1 inhibitor responsive. The induction signaling driving cystogenesis may be mediated by extracellular vesicle trafficking.

Introduction:

Tuberous sclerosis complex (TSC) is caused by mutations in either the *TSC1* or *TSC2* genes and affects over one million patients world-wide (24, 33, 73). Over 80% of young patients and all postmortem samples (mean age 30 years (89)) were found to have renal disease. Renal cystic disease is detected by MRI in ~50% of TSC patients, though the pathogenesis is not well studied. Premature decline of glomerular filtration rate (GFR) occurs in ~40% of patients with TSC (8) and can occur in the absence of overt angiomyolipomata bleeding or interventions and is, at least in part, due to renal cystic disease.

TSC renal cystic disease exhibits five distinct patterns (6, 7) and involves the mechanistic target of rapamycin complex 1 (mTORC1) signaling pathway. The mTORC1 signaling pathway integrates intra- and extracellular information to regulate cellular metabolism, translation, growth, proliferation, autophagy, and survival and is critical for organogenesis and organ maintenance. The TSC proteins directly regulate mTORC1 activity and influence downstream processes, including renal development, homeostasis and malignancy. Although the TSC proteins play a pivotal role of in cell biology, how their regulation of the mTORC1 pathway is involved in cystogenesis is not known.

The etiology of another common TSC renal lesion, angiomyolipomata, is thought to rely on a somatic mutation mechanism that disables the functional copy of the affected *TSC* locus leading to clonal proliferation of cells lacking TSC-mediated regulation of the mTORC1 pathway (57). There are multiple interactions between mTORC1 signaling and candidate cystogenic mechanisms. Investigation of both *Tsc1*- or *Tsc2*-associated renal cystic disease mouse models directly (1, 61, 101) or indirectly (21) demonstrated that cystogenesis is attributable to specific nephron segments, and all tubular segments have been implicated in *Tsc* cyst formation (95). The identification of the cell of origin for renal cysts is complicated by the tubular epithelial capacity to undergo dedifferentiation during repair/regeneration, and restorative processes that recapitulate renal developmental processes (30). Interestingly, all mouse model studies that examined both mTORC1 activity and targeted cells exhibit a mismatch between exhuberant cystic phospho-S6 expression, and the much lower percentage of cells exhibiting loss of Tsc expression (1, 61, 101).

Published mouse Tsc models are commonly reported to be born with normal kidneys but cystogenesis progresses with age. One such model has been reported to be associated with a potassium excretion defect (21). Early investigation revealed that the majority of renal cysts maintain their *Tsc* locus integrity (61, 98), as loss of heterozygosity was found in a striking minority of cystic epithelial cells. This is similar to human TSC renal cystic disease, where human cysts continue to express tuberin and hamartin, and this contrasts with a very different mechanism in the formation of angiomyolipomata, which show an inactivating mutation and loss of *Tsc* gene expression (13). Such a low percentage of loss of heterozygosity is seen also in *PKD1* associated autosomal dominant polycystic kidney disease, suggesting that such cystic disease may represent a unique disease mechanism (3, 14) .

To build on these initial studies of *Tsc*-associated renal cystic disease in the mouse model system, we employed two newly developed mouse *Tsc*-renal cystic disease models, one that disrupts the *Tsc2* gene in renal principal cells, and the other that disrupts the *Tsc1* gene in renal pericytes. These models suggest that, similar to renal development, a tissue induction or reprograming phenomenon occurs such that cells with an intact Tsc gene adopt *Tsc* mutant cell phenotypes, defining a new and distinct mechanism of disease from that reported for angiomyolipomata development. These finding help explain the discrepancies between disease tissue architecture and persistence of TSC protein expression and demonstrate that genetically normal, TSC-intact cells are induced in large part to participate in cystogenesis.

Results:

Mouse Models of Tsc Cystic Kidney Disease

The most severe forms of human TSC cystic disease include polycystic variety associated with the contiguous gene syndrome (16, 48) and microcystic disease (6). There is a well-established association between primary cilia defects and the development of renal cystic disease. To create a mouse model that would phenocopy these severe TSC renal diseases, we targeted the primary cilia expressing renal collecting duct principal cell. To achieve this , we disrupted the floxed *Tsc2* gene in the kidney using by aquaporin-2 (*Aqp2*) promoter to drive Cre-recombinase (*Aqp2Cre*) expression. By crossing these *Aqp2Cre* transgenic mice with floxed *Tsc2* mice, we generated the *Aqp2CreTsc2* mouse. These mice have relatively normal kidneys at birth but develop florid cystic disease by week 11 (Figure 1A). At 11 weeks, mice that do not

harbor the *Aqp2Cre* have kidneys that are 1 cm long, while mice that do express the recombinase (*AqpCreTsc2*) have kidneys that are twice this length and have visible cysts on the surface (Figure 1A).

Coronal sections of the diseased kidney (Figure 1B) revealed a cortical cyst pattern. The cortical cysts were not matched by medullary cysts over time, despite the fact that the principal cell density increases along the collecting duct into medulla. The *Aqp2CreTsc2 mice* had a reduced median survival of 147 days and did not develop angiomyolipomata.

We posited that there is a causal relationship between angiomyolipomata and TSC renal cystic disease, so our second model focused on cystic disease caused by disrupting the *Tsc* axis in a putative cell of origin of angiomyolipomata. Recent evidence suggests that angiomyolipomata arise from a subpopulation of renal vascular pericytes (87); therefore, we used the *Ren1cCre* to disrupt the floxed *Tsc1* allele (*Ren1cCreTsc1*). Although *Ren1cCre* recombinase is expressed in the renal pericyte compartment, the animals most often develop cystic disease. The disease appeared to be more commonly unilateral, without a side preference. These mice also had a 25% reduction in their litter sizes ($p=0.02$ via Fisher's Exact Test), suggesting that bilateral disease compromised survival. The affected kidney in these animals was larger than the grossly unaffected contralateral kidney (Figure 1C). Histologically the affected kidney exhibited significant renal cyst epithelial cell enlargement, some cystic epithelia were hyperplastic, and occasional prominent nucleoli were identified (Figure 1D). These mice grew at a normal rate, with normal body weight and no apparent gross developmental defects, but showed lethality at a median of 85 days, essentially during adolescence.

Tsc Genes in Cystic Epithelium Remain Intact

Because previous murine models of *Tsc* renal cystic disease do not show convincing 'second hit' mechanism for the *Tsc* renal disease (61, 98), and human TSC-associated cysts express hamartin and tuberin (13), we wished to ascertain the *Tsc* gene integrity in cystic epithelium in our models. To assess if the cysts exhibited the loss o; heterozygosity as described in the angiomyolipomata, we used immunohistochemistry as well as a genetic analysis for *Tsc2* recombination in the cysts from the *Aqp2CreTsc2* mice. To validate the results, we used two different commercially available antibodies with publicly available validation for tuberin (20, 70) western blot analysis and a polymerase chain reaction assay to probe for recombination by the maintenance of a *Lox*P2 site. We assayed one of the antibodied by western blot to assure that we

got similar results to reported data (Cell Signaling, see Table 1). To generate target cell lines, we used a parental cell line from mouse inner medullary collecting ducts (IMCD), and isogenic cell lines that were modified to disrupt either *Tsc1*(T1H and T1J) or *Tsc2* (T2H and T2J) using CRISPR/CAS9 technology (Figure 2A). The effect of harmartin expression on tuberin expression has previously been reported (5). We identified tuberin expression in cystic epithelium with both antibodies. Furthermore, we found that the expression of tuberin was not seen in the less common cell that expressed aquaporin-2 (Figure 2B). The cortical expression and cysts was distinct from the expression in the medulla, where again tuberin or aquaporin-2 expression were mutually exclusive, but aquaporin-2 expressing cells were much more numerous. To genetically assess *Tsc2* gene recombination, we used a PCR approach to see if the *lox*P2 site was retained. The cystic epitheium demonstrated the same size band comparing DNA from liver and cyst wall eithelium (Figure 2C). Sequencing these bands demonstrated that they retain the sequence and had not undergone Cre-mediated recombination (Figure 2D).

These results lead us to probe for recombination in the cysts of the *Ren1cCreTsc1* mice. The cystic disease in the *Ren1cCreTsc1* model has more numerous and smaller cysts (Figure 1C and D), so directly obtaining cystic tissue would be more prone to contamination by DNA from non-cystic cells. Instead, we probed for *Ren1cCreTsc1* cystic *Tsc1* deletion by breeding the *Ren1cCreTsc1* onto the 'confetti' reporter background (Figure 3A-D). We utilized this technique to evaluate genetic status of the cysts in *Ren1cCreTsc1* affected kidneys. While we identified clear fluorescence in arterioles, indicating Cre-mediated recombination, we could not identify fluorescence in the cystic epithelium in any of the slides screened. Thus, like in the *Aqp2CreTsc2* model, the genetic evidence corroborates the immunohistochemical evidence that *Tsc* genes were intact in the cysts in these models.

Cellular Composition of Tsc Cystic Epithelium

To characterize the renal cystic epithelial and gain insight into the cystogenic pathways and/or mechanisms at play in these models, we used both lectin and immunofluorescent staining. Multiple cystic epithelia histochemically stained diffusely with *Dolichos biflorus* agglutinin (DBA), which predominantly labels the collecting duct, while a few cysts were not stained (Figure 4A). To identify the nephron segment(s) and the cell types comprising the cyst epithelium, single and double immunofluorescence labeling experiments were performed using antibodies against transporters, channels or molecules with specific nephron segment

distribution. We first probed for principal cells labeling in renal collecting ducts of wild-type (left panel) and *Aqp2CreTsc2* mice (right panel) using anti-aquaporin-2 (AQP-2) immunofluorescent staining (Figure 4B). AQP-2 expression was present in non-cystic tubules but surprisingly was absent in cyst epithelial cells in *Aqp2CreTsc2* mice (Figure 4B, right panel). The labeling in wild-type kidney is consistent with AQP-2 expression in principal cells (Figure 4B, left panel). A double immunofluorescence labeling with AQP-2 (green) and H^+-ATPase (red), a marker of intercalated cells, in a normal mouse kidney shows multiple principal cells (AQP-2 positive) interspersed with intercalated cells (H^+-ATPase positive) in wild-type cortical collecting ducts (Figure 4C). Using AQP-2 and H^+-ATPase double immunofluorescence staining in the *Aqp2CreTsc2* kidney revealed an age-dependent change. Figure 4D demonstrates double immunofluorescent labeling with AQP-2 (green) and H^+-ATPase B subunit (red) in kidneys of 5 weeks (left panel) and 11 weeks old (right panel) *Aqp2CreTsc2* mice. As shown, 5 weeks old *Aqp2CreTsc2* mice exhibit early signs of cyst development in their kidneys (depicted with the letter "C"). Several principal cells and numerous intercalated cells are present in cyst epithelium as verified by the expression of AQP-2 (green) and H^+-ATPase (red), respectively, in distinct cells. Interestingly, the H^+-ATPase-positive cells (white arrows) are more abundant compared to AQP-2 positive cells (yellow arrows) in cyst epithelium. Kidneys of 11 weeks old *Aqp2CreTsc2* mice (Figure 4D, right panel) show more frequent and larger cysts in the cortex and display robust and almost uniform expression of H^+-ATPase along the apical membrane of cyst epithelium. There are very few AQP-2 positive cells in cyst epithelia in 11 weeks old *Aqp2CreTsc2* mice (Figure 4D, right panel). These changes are consistent with the proliferation of A-intercalated cells and gradual disappearance of principal cells in cyst epithelium.

We were intrigued by the H^+-ATPase in the intercalated cells because in the kidney, the prorenin receptor (PRR) co-localizes with H^+-ATPase in intercalated cells and functions as a receptor for renin. Pro-renin, a critical chaperone for the assembly of H^+-ATPase subunits, regulates cell proliferation via the mitogen activated protein kinases ERK1/2 cascade and is a crucial component of Wnt pathways (19, 25, 52, 68, 74, 75, 81, 82). There is robust and uniform PRR expression on the apical membrane of cyst epithelium in 11 weeks old *Aqp2CreTsc2* mice (Figure 4E, right panel) and parallels the H^+-ATPase expression pattern, as does the PRR expression in the 5-week old *Aqp2CreTsc2* mice (Figure 4E, middle panel). PRR expression in control animals is shown for comparison (Figure 4E, left panel).

To determine whether other nephron segments or tubular cells contribute to cyst epithelium, we performed double labeling with the Na^+:HCO_3^- cotransporter NBC-e1 (red fluorescence), which primarily labels the basolateral membrane of proximal tubule and thick ascending limb of Henle (TALH), and H^+-ATPase (green fluorescence), which is strongly expressed in intercalated cells. NBC-e1 (Figure 4F, right panel) was detected in normal, non-cystic nephron segments, but was completely absent in cyst epithelial cells in adult *Aqp2CreTsc2* mice. The H^+-ATPase showed a very strong and uniform labeling in cyst epithelial cells (Figure 4F, left panel). The Na-Cl cotransporter NCC, a marker of distal convoluted tubule, and pendrin, a marker of B-intercalated cells, did not show any labeling in cyst epithelia (Data no shown). Additional staining for the sodium-hydrogen exchanger-3, a marker of proximal tubule and thick ascending limb of Henle, failed to identify this transporter in the cystic epithelium (Data not shown). The Na^+-K^+ ATPase showed normal expression in non-cystic nephrons but displayed minimal basolateral labeling in cyst epithelial cells (Data not shown). Cystic epithelium does express type A intercalated cell localization of H^+-ATPase on the apical surface and AE-1 on the basolateral surface (figure 4G).

Because we identified a new cystogenic mechanism, we wished to compare Tsc renal cystic disease to *Pkd1* renal disease. Kidney sections from a *Pkd1* mutant mouse (generated using a PAX8 cre mouse and a generous gift from Dr. Stephen Somlo) were examined for the expression of H^+-ATPase and AQP-2. Double immunofluorescence studies demonstrate that in *Pkd1* mutant mice, cysts originating from the cortical collecting duct contain both principal cells and intercalated cells (Figure 4H).

We use female mice and X-chromosome inactivation to assess if type A intercalated cells in cystic epithelia results from expansion of single cell (i.e monoclonal) or multiple cells (polyclonal). Figure 4I shows a greater than 25% reduction in methylated-*pgk1* locus on the X chromosome in cortical tissues of wild type and cystic epithelia of *Aqp2CreTsc2 female* mice, more strongly supporting a polyclonal nature of the cystic epithelium.

The absence of labeling with AQP-2, pendrin, NBC-e1, NCC or NHE-3 antibodies in renal cystic epithelium of *Tsc2*-specific knockout mice indicated that the cysts were not comprised of the targeted principal cells, nor the B-intercalated cells, proximal tubule cells, thick ascending limb of Henle cells or distal convoluted tubule cells. The H^+-ATPase apical location correlated very well with the cyst fluid pH that ranged from 5-5.6, and was most compatible with the cystic

epithelium exhibiting an A-intercalated cell phenotype. This cell of origin is also important as the intercalated cells do not express a primary cilia, and the cysts in out model also fail to express significant cilia (Figure 5).

Because of the novel cystogenic process in the *Aqp2CreTsc2* model, conducted similar studies in the *Ren1cCreTsc1* model. As with the *Aqp2CreTsc2* mouse model, the DBA staining was detected in most but not all cysts in the *Ren1cCreTsc1* model (Figure 6A). Similar to *Aqp2CreTsc2* mice, the *Ren1cCreTsc1* mice did not show any expression of AQP-2 on the apical membrane of cyst epithelia (Figure 6B, right panel). The expression of AQP-2 in cortical collecting duct in a normal kidney is shown for comparison (Figure 6B, left panel). The double labeling with NBC-e1 and H^+-ATPase revealed a strong and uniform expression of H^+-ATPase on the apical membrane of cyst epithelia but did not demonstrate any labeling with NBC-e1, a marker of proximal tubule and thick ascending limb of Henle cells (Figure 6C, right panel). The expression of NBC-e1 in normal kidney **(**Figure 6C, left panel**)** and in non-cystic kidney tubules in *RenCreTsc1* is shown (Figure 6C, right panel). The cystic epithelia showed a strong and uniform expression of PRR on their apical membrane (Figure 6D). The double labeling with Na^+-K^+ ATPase and NBC-e1 indicates basolateral expression of Na^+-K^+-ATPase in multiple nephron segments in normal kidney (Figure 6E, first and third panels). In *RenCreTsc1* mice, the Na^+-K^+-ATPase exhibits strong basolateral expression in non-cystic tubules and mild expression in cystic epithelia (Figure 6E, fourth panel). The basolateral Na^+:HCO_3^- cotransporter NBC-e1 shows no expression in cystic epithelia but shows normal expression in non-cystic epithelia (Figure 6E, second panel). There was no labeling with NCC, pendrin, or NHE-3 antibodies in renal cysts, indicating the lack of B-intercalated cells, principal cells, distal convoluted tubule cells, proximal tubule cells or thick ascending limb of Henle cells in cyst epithelium adult *Ren1cCreTsc1* mice.

To better establish the role of intercalated cells in cyst epithelia proliferation in these *Tsc* knock out mice, we performed double labeling with H^+-ATPase and proliferating cell nuclear antigen (PCNA) in kidneys of *Aqp2CreTsc2* and *Ren1cCreTsc1* mice (Figure 6F). Similar staining was performed on kidneys from *Pkd1* mice (Figure 6F, fourth panel). For comparison, PCNA labeling in wild type mice is shown (Figure 6F, first panel).

As observed in multiple high magnification images, wild type mice showed very few PCNA positive cells per each field (Figure 6F, first panel). However, the H^+-ATPase-expressing

epithelial cells lining the cysts in *Aqp2CreTsc2* mice showed numerous PCNA positive cells **(**Figure 6F, second panel**)**. Similarly, the cyst epithelium in *RenCreTsc1* mice showed many H^+-ATPase expressing cells that also displayed positive staining for PCNA (Figure 6F, third panel), a pattern very similar to *Aqp2CreTsc2* mice. The cells lining the cysts in *Pkd1* mice showed a relative increase in the number of PCNA positive cells in cyst epithelium as compared to wild type mice (Figure 6F, fourth panel). However, the number of PCNA positive cells in *Pkd1* mice was significantly less than that in *Aqp2CreTsc2* or *Ren1cCreTsc1* mice. Further, only a minority of PCNA-expressing cells showed co-labeling with H+-ATPase (Figure 6F, fourth panel).

Our results consistently indicate that A-intercalated cells with an unrecombined *Tsc* gene are induced or reprogramed to form cysts in both *Aqp2CreTsc2* or *Ren1cCreTsc1* models. Basically, the loss of heterozygosity in the small number of cells would be combined with a gain of function mechanism that affects the surrounding genetically unrecombined cells and tissue. The significant difference in A-intercalated cell expansion in *Tsc* knockout mice vs. *Pkd1* mice (results above) highlights the difference in the role of A-intercalated cells in these two kidney cystic models.

mTORC1 Inhibition Response of Genetically Normal Cystic Cells

The examination of these two very different murine models of real cystic disease suggest the presence of a common mechanism involving the adoption of a *Tsc* mutant phenotype in genetically normal cells that is induced by the loss of *Tsc* function in a small number of adjacent cells. These observations have important implications as far as mechanism of disease and possible response to mTORC1 inhibitors are concerned. Such inhibitors are effective and are approved for the treatment of TSC-associated renal angiomyolipomata (9, 10), subependymal giant cell astrocytomas (35), and lymphangioleiomyomatosis (10, 60) and possibly small cysts in humans (85). However, unlike the angiomyolipomata in human, these murine models of cystic renal disease involve non-mutant epithelium (36).

To determine if mTORC1 activation was involved in this new cystogenic mechanism, we first examined the phospho-S6 staining in the *Aqp2CreTsc2* cystic tissue. There was a uniform increase in phospho-S6 staining of the cystic epithelium (Figure 7A). There was also a significant increase staining for phospho-S6 in the *Ren1cCreTsc1* cystic epithelium (Figure 7B). These results support the involvement of the mTORC1 pathway in this novel mechanism of cystogenesis, even though the *Tsc* genes are intact. To test whether inhibiting the mTORC1 axis

could be therapeutic, we treated animals from both models with rapamycin and used survival as a readout of effect. Administration of rapamycin for the *Aqp2CreTsc2* and the *Ren1cCreTsc1* significantly prolonged the animal survival (Figure 7C and D).

Implications for Human Disease

The polycystic and the microcystic kidney variety of TSC lead to loss of renal function by adolescence or young adulthood. These forms of TSC renal cystic disease are in the most need of therapeutic intervention. Given the unexpected results reported here, we wished to determine if human disease exhibited a similar pathology and response to mTORC1 inhibition. To test the staining characteristics of human TSC renal cystic disease associated tissue, we used a nephrectomy specimen for the polycystic kidney disease phenotype (Figure 8A). Similar to the mouse models, the apical epithelium revealed H^+-ATPase staining (Figure 8B) and demonstrated findings again consistent with cystogenic participation of A-intercalated cells. A similar finding was also revealed in the staining of the microcystic disease biopsy (Figure 8C).

While the A-intercalated cells appear to be involved in human TSC renal cystic disease, therapeutic response to mTORC1 inhibition is not clear. Although one publication suggested a possible response of mild TSC cortical cystic disease to mTORC1 inhibitor therapy (85), it is not clear that mTORC1 inhibition is useful for severe forms of TSC renal cystic disease. We examined patients with the focal and cortical cystic variants of TSC (7) who were on an mTORC1 inhibitor clinically and found that they also respond to mTORC1 inhibitors by reducing their cystic burden Figure 8 D&E). Five TSC patients were identified that were placed on an mTORC1 inhibitor with either focal or cortical cystic kidney disease for at least one year. Total renal cystic count of the cysts were performed prior to therapy and after at lest one year, and a significant reduction ($p<0.025$ ratio paired t-test) of cystic burden was identified (Figure 8F).

Possible Role of Extracellular Vesicles in Disease Phenotype Induction

To begin to explore possible mechanisms for the phenotypic induction that we described in this manuscript, we tested the probability that extracellular vesicles may be involved. This exploration was based on several reasons. First, such extracellular vesicles are a prominent component of renal pathophysiology (69), and their release is stimulated by ER stress (51) such as that which occurs in cells with a disrupted TSC (86). Second, extracellular vesicle release as

well as fusion are known to be increased in an acidic extracellular environment (59, 62), and the cyst fluid in the *Aqp2CreTsc2* model has a pH=5.0, likely as a result of increased H^+-ATPase expression and activity in the luminal aspect of the cyst. Lastly, increased release of extracellular vesicles has also been shown to occur in states of hypoxia or conditions of increased HIF1α production (55), such as that seen with increased mTORC1 activity driving increased HIF1α (27). In early cysts we were able to identify extracellular vesicles in the cyst lumen (Figure 9A), and could also detect either vesicle shedding or fusion with the apical epithelial cell (Figure 9B). To test if these vesicles could mediate the increased mTORC1 activity, we developed a cell culture experiment using IMCD conditioned media by itself, or isolated extracellular vesicles from either one or three milliliters of conditioned media in experiments using intercalated cells (M1 cortical collecting duct cell line) as a target (Figure 9C). This cell line does not express primary cilia, and morphologically this cell is most compatible with an intercalated cell line (90). We used western blot analysis of phospho-S6 as a read out of mTORC1 activity.

We used a parental IMCD cells, and isogenic cell lines that were modified to disrupt either *Tsc1* or *Tsc2* using CRISPR/CAS9 technology (Figure 2A). To examine the possible transfer mTORC1 pathway activity from the IMCD cells to the intercalated cells by extracellular vesicles, we determined the phosphorylation of S6 kinase of M1 cell lysates after 24 hours of exposure to isolated extracellular vesicles (Figure 9D). Comparing the phospho-S6 band to the S6 band, there is a significant increase in the phospho-S6/S6 ratio with the higher dose of extracellular vesicles derived from the Tsc2 deficient IMCD cells (Figure 9D).

Discussion:

We report a new cellular cross-talk mechanism resulting in tuberous sclerosis renal cystogenesis. A fundamental feature of this mechanism involves a small population of *Tsc* mutant renal principal epithelial cells or pericytes that induce or reprogram genetically normal A-intercalated cells to upregulate their mTORC1 activity, proliferate, and form renal cysts (Figure 10). Similar microenvironmental effects that increase malignant potential have implicated extracellular vesicles (102). Extracellular vesicles derived from *Tsc1*-null cells transform the phenotype of neighboring wild-type cells *in vivo* such that the wild-type cells became functionally similar to *Tsc1*-null cells (64), a phenomenon sometimes termed “phenotypic

spreading". Such extracellular vesicles have been demonstrated to affect renal tubular changes in a von Hippel Lindau zebrafish model (96). This extracellular vesicle initiating event has appeal because as the cyst develops, the tubular lumen increases in diameter and exponentially reduces the flow, thus increases the time for the extracellular vesicles to interact with intercalated cells. As the cysts enlarge, they detach from the tubule (40), potentially entrapping the extracellular vesicles in the closed cystic space. The intercalated cells with the increased mTORC1 activity likely also participate in the process both in shedding and uptake of the vesicles. This effect also may be mediated through a cellular reprogramming mechanism that induces a sustained change in cellular activity in a paracrine-like (principal or pericyte to intercalated cell) or autocrine-like fashion (intercalated to intercalated cells) (71). Such a programing effect has been shown *in vitro* using cells derived from a TSC patient angiofibroma (49).

Our mouse models and human samples demonstrate a significantly increased preponderance of H^+-ATPase positive A-intercalated cells and disappearance of principal and B-intercalated cells in the cystic epithelium (Figures 4 and 6). The vacuolar H^+-ATPase is ubiquitously expressed in the membranes of intracellular organelles, including lysosomes, where it plays a crucial role in their acidification. The H^+-ATPase is also found in the plasma membranes of certain specialized cell types, including kidney A-intercalated cells, epididymis, osteoclasts, and certain tumor cells (11, 15, 17, 22, 37, 58). H^+-ATPase plays an important role in stimulating chloride secretion via apical chloride channels in the collecting duct (34). These results support the presence of a mechanism that drives the progressive expansion of A-intercalated cells and the disappearance of principal cells similar to what is described for the differentiation of ionocytes and keratinocyte maintenance in zebra fish embryos (47).

Communication between H^+-ATPase and mTORC1 is implicated in reciprocal amplification of their functions. A significant role for H^+-ATPase in mTORC1 regulation and translocation to the lysosomal membrane has been demonstrated in several conditions (103). The H^+-ATPase undergoes amino acid dependent interactions with the Ragulator complex, which recruits mTORC1 to the lysosomal membrane during amino acid sensing (54). Genetic deletion of structural components of H^+-ATPase suppressed amino acid-induced S6K phosphorylation in *Drosophila* and mammalian cells (103). Functional inhibition of H^+-ATPase activity by chemical inhibitors or by RNAi abrogated mTOR translocation to lysosomes upon amino acid stimulation (103). These results demonstrate that amino acids activate mTORC1 by stimulating its

translocation to the lysosomal membrane where it forms a super-complex involving the H^+-ATPase (103), suggesting that H^+-ATPase is part of the amino acid–induced signaling pathway that culminates in mTORC1 activation (67).

The reciprocal effect of mTORC1 regulating H^+-ATPase also has been identified because mTORC1 up-regulated the expression of H^+-ATPases in immortalized mouse embryo fibroblast (MEF) cells from *Tsc2*$^{-/-}$ mice (67). In addition, mTORC1 facilitates the assembly of V0 and V1 domains of H+-ATPase. These results (54, 66, 67, 79, 103) indicate that TSC gene deletion enhances H^+-ATPase expression via mTORC1, which, requires H^+-ATPase for sustained activity. This amplification loop may play a significant role in the dysregulation of cell growth, expansion of A-intercalated cells and cystogenesis subsequent to initial signals by TSC mutant cells. Interestingly, our results demonstrate that, despite this new disease mechanism, mTORC1 inhibition can lead to improvement in the patients suffering from TSC renal cystic disease.

TSC cystogenesis has some significant differences with reported pathogenesis in ADPKD, where kidney cysts may originate from multiple nephron segments but predominantly arises from the collecting duct (39, 41). Fluid accumulation in ADPKD cysts is caused by active chloride secretion via AVP-stimulated cAMP-mediated CFTR activation (26, 91). A prostaglandin E2 (PGE2)-induced chloride secretion mechanism in collecting duct cells involving cAMP-CFTR- and/or calcium-dependent Cl^- channel also has been identified (72). Within cysts originating from collecting duct in ADPKD, both intercalated and principal cells are present and principal cells play an important role in fluid secretion (26, 91). Contrary to cysts in ADPKD, our studies using two disparate models demonstrate that cyst epithelia in adult *Tsc1- and Tsc2-KO* mice is almost exclusively comprised of A-intercalated cells, with very few or no principal cells. As such, intracellular cAMP-activation by AVP may not be a dominant driving force in cyst fluid accumulation and expansion in TSC. Further, whereas our studies clearly demonstrate a uniform and strong expression of apical PRR in the cyst epithelia in *Tsc-2* KO mice, PKD cysts show a basolateral localization of PRR in principal cells (78). The cystic mTORC1 activated ADPKD cell could still utilize the activation loop involving the basolateral H^+-ATPase, but the cells involved and H^+-ATPase location would be different than that for the TSC cystogenesis.

The mTORC1 activation may involve the cystoprotein polycystin-1 (PC-1) in explaining cystogenesis, and may help explain why the *PKD1/TSC2* contiguous gene syndrome has such a

severe phenotype. mTORC1 activity negatively regulates the biogenesis of PC-1 and proper trafficking of the PC-1/2 complex to cilia (Figure 7B). While PC-1 is located on the cilia of principal cells, it is also found on other cell membranes including intercalated cells (53, 80), and is strongly expressed on extracellular vesicles (45). Genetic interaction studies have revealed that PC-1 downregulation by mTORC1 leads to cystogenesis in *Tsc1* mutants (65). These findings potentially explain the severe renal manifestations of the *PKD1/TSC2* contiguous gene syndrome. This mechanism also helps explain the Eker rat model described by the Walker laboratory, that developed severe cystic disease and gave rise to the cell line EKT2 (18). It is intriguing, given the inputs of von Hippel Lindau protein (31, 83) and folliculin (42) proteins into mTORC1 activity, to posit that these phakomatoses may also arise from a similar mechanism as TSC renal cystic disease.

The disease phenotypic adaption mechanism identified in our animal models complicates the mechanistic understanding of autosomal dominant disease expression. For autosomal dominant polycystic kidney disease, both somatic mutation (second hit") and haploinsufficiency mechanisms have been put forward. For TSC renal disease, somatic mutation has been favored and has been shown for angiomyolipomata (43), but this is not present in the brain tubers or renal cysts (13, 44). Human TSC cystic epithelium continues to express the TSC gene products, hamartin and tuberin (13). In TSC renal cystic disease, both loss of heterozygosity in the inciting cell, and an induced or reprogramed gain of function in the genetically normal cyst forming epithelium, is involved. The cystic phenotype may depend on the presence of A-intercalated cells. The *Aqp2CreTsc2* renal medullary collecting duct cells are devoid of cysts despite their lack of tuberin expression. The cystic disease may require the intercalated cell plasticity for disease phenotype manifestation ( ). This novel mechanism better explains the TSC brain tubers. The genetically abnormal giant cell could use extracellular vesicles to reprogram normal cells to participate in the tuber formation, as supported by detailed genetic analysis of tubers (23) It is intriguing that mutant pericytes that likely give rise to the TSC-associated renal angiomyolipoma (87) could also be involved in TSC renal cystogenesis. Pericytes that have lost TSC gene function may be responsible for altered blood brain barrier function giving rise to the tensor weighted imaging findings in TSC (2, 32, 50) and may participate in inducing subependymal giant cell astrocytoma formation, a TSC tumor also sometimes identified without loss of heterozygosity (12, 63, 76), possibly through this

extracellular visicle mechanism. The expansion of A-intercalated cell as well as potential role for extracellular vesicles in many aspects of TSC renal cystic disease manifestation offers new therapeutic opportunities for intervention in this disease.

Materials and Methods

Animal Procedures

Ren-1c-Cre mice were generated in the laboratory of K.W. Gross (38). Floxed *Tsc1* mice (stock #005680; (56)) and Floxed Tsc2 mice (stock #027458) were obtained from The Jackson Laboratory AqpCre mice and 'Confetti' mice were also obtained from The Jackson Laboratory. The 'Confetti' reporter uses the Brainbow2.1 cassette inserted into the *Rosa26* locus, where it is driven by the *CAGG* strong promoter. The reporter system is activated by excision of a floxed stop sequence by the Cre recombinase. The Brainbow reporter cassette contains two inverted repeats of fluorescent reporter genes: GFP paired with inverted YFP, and RFP paired with inverted CFP. The loxP sites within the construct are in direct and inverted orientations to facilitate loss of the floxed stop module and expression of one of the reporter pairs. The remaining reporter pair can continue to 'flip' into the active orientation for one of the two inverted reporters while Cre activity remains present, resulting in bi-colored cells, and will be locked into one or the other orientation when Cre activity stops (88).

All animal research was done in adherance to the NIH Guide for the Care and Use of Laboratory Animals. These mice were crossed to generate offspring that were heterozygous for the floxed allele, and were either heterozygous or wild-type at the *Cre* allele. These mice were then intercrossed to generate knockout mice (*Tsc1*$^{fl/fl}$; *Ren-1c-Cre*$^{Tg/+}$), wild-type mice (*Tsc1*$^{+/+}$; *Ren-1c-Cre*$^{+/+}$) and controls for the floxed allele (*Tsc1*$^{fl/fl}$; *Ren-1c-Cre*$^{+/+}$), *Cre* allele (*Tsc1*$^{+/+}$; *Ren-1c-Cre*$^{Tg/+}$). A similar strategy was used for the AqpCre lineages. Animals were housed in a 12 hour dark-light cycle according to protocols approved by the University of Tennessee Health Science Center Institutional Animal Care and Use Committee. For rapamycin injections, drug was dissolved in vehicle (5.2% PEG 400/Tween 80) and injected at 3 mg/kg three times per week starting at weaning (21 days of age).

Perfusions

Three clear plastic tubes were connected by three-way stopcock to a peristalic pump. The ends of two tubes were placed in either 0.9% saline or 10% neutral buffered formalin. A 30 ½ G needle was attached the the end of the third tube. The formalin tube was filled to the stopcock and the saline tube was allowed to flow from the needle at a rate of 0.01 mL/s. Prior to perfusion, mice were anesthetized twice, first with isoflurane in a drop until their heartbeat slowed to 1 beat per second, followed by an intraperitoneal injection of 0.8 mL/20g body weight of Avertin. Once there was no reaction to painful stimuli (e.g. toe pinch), the chest cavity was opened and the diaphragm cut. With the heart exposed, the apex of the left ventrical was punctured with the 30 ½ G needle attached to the perfusion liquid tubing and the aorta was cut. Mice were perfused with 0.9% saline, followed by 10% neutral buffered formalin for 10-12 minutes each. Dissected tissues were stored in formalin overnight, then in 70% ethanol (Pharmaco-Aaaper) until processing.

Histology and Immunohistochemistry staining

Tissues were processed with the following washes: 30 min in 75% ethanol, 2 x 75 min in 95% ethanol, 3 x 1h in 100% ethanol, 2 x 30-60 min in Citrosolv (Fisher Scientific) and 2 x 1h in Paraplast XTRA (Sigma-Aldrich), with an additional final incubation overnight in Paraplast XTRA under vaccuum). Tissues were embedded into blocks using Paraplast XTRA paraffin (Sigma-Aldrich) in a Thermo Shandon Histocentre 3 paraffin embedding station. For Immunohistochemistry, the kidneys from the knockout mice (*Tsc1*$^{fl/fl}$; *Ren-1c-Cre*$^{Tg/+}$) and wild-type mice were prepared in 10% formalin fixed, paraffin embedded. Tissue blocks were cut to 8μm sections. Immunohistochemical stains were carried out using the The VECTASTAIN® Elite® ABC HRP Kit (Vector Laboratories, Burlingame, CA, USA) with DAB (3,3-diaminobenzidine) as the chromogen (Vector Laboratories, Burlingame, CA, USA). For antibodies used, please see table 1). All the sections were counterstained with Gill2 Hematoxylin (Fisher Scientific, Hampton, NH).In every case, formalin-fixed tissue was subjected to heat-induced antigen retrieval. Endogenous peroxidase activity was blocked with 3% H_2O_2. Avidin/Biotin Blocking Kit (Vector Laboratories, Burlingame, CA, USA) was used to block all endogenous biotin, biotin receptors, and avidin binding sites present in tissues. For all immunohistochemical studies, more that 95% of the slide had the reported pattern of staining.

Immunofluorescence labeling

Single and double immunofluorscence labeling was performed using established protocols (4, 97, 99, 100). Briefly, animals were euthanized with an overdose of pentobarbital sodium, and kidneys were perfused with saline followed by 4% paraformaldehyde removed, cut in tissue blocks, and fixed in 4% paraformaldehyde solution overnight at 4^{o}C. The tissue samples were preserved in 70% ethanol, paraffin embedded and 5-µm sections. For staining, after rehydration and sodium citrate antigen retrieval sections were incubated overnight at 4^{o}C with the primary antibodies (Table 1). Sections were then washed in PBS and incubated with Alexa Fluor conjugated secondary antibodies (Invitrogen, Eugene, OR) for one hour at room temperature. Sections were washed in PBS, dried and cover slips were applied using Vectashield Mounting Medium (Vector Labs, Burlingame, CA).

Immunofluorescence microscopic analysis of tissue sections was performed on a Zeiss Axio Imager.M2 Microscope. Images were acquired using Ziess Axiocam 506C digital camera. Images were processed using Zeiss Zen 2012 software. For each figure, the settings for each panel were identical. For all immunofluorescence studies, more that 95% of the slide had the reported pattern of staining.

Multispectral imaging of kidney tissue

Kidney from *Ren-1c-Cre*, *fl-Tsc1* or *fl-Tsc2*, Confetti were excised immediately after euthanasia of the mice. One-third part of both kidneys were cut into ~1mm thick sections. Individual sections were squashed to ~20 nm thickness between two glass slides. The tissue was imaged on an inverted Nikon Eclipse Ti fluorescent microscope equipped with a Nuance FX multispectral camera. The four fluorescent proteins encoded by Confetti were identified in the tissue based on reference spectra for each proteins. The remaining kidney parts were fixed in paraformaldehyde, embedded in OCT and cut in a cryotome into 5-µm thick sections. The sections were analyzed by multispectral imaging as done for the fresh tissue squashes.

Development of Tsc mutant cell lines

We disrupted either the *Tsc1* or *Tsc2* genes in principal cells using CRISPR/Cas9 genome editing as previously described (84). A CRISPR plasmid with constitutive green fluorescent protein (GFP) expression and containing guide RNA sequences was constructed by the Cincinnati Children's Hospital Medical Center (CCHMC) Transgenic Animal Genome Editing Core Facility. The guide RNA sequences were selected using algorithms in Benchling.com for on-

target (28, 29) and accounting for off-target (46) sites. For both the *Tsc1* and *Tsc2* genes, exon 4 was targeted. We used Lipofectamine 3000 (Thermo Fisher Scientific) to transfect mIMCD-3 cells with these plasmids. At 2 days after transfection, single GFP-positive cells were sorted into separate wells for expansion (FACSAria II, BD Biosciences, San Jose, CA, located at the CCHMC Research Flow Cytometry Core). After expansion, extracted genomic DNA (GeneJET Genomic DNA Purification Kit, catalog no. K0721, Thermo Fisher Scientific) was used in a polymerase chain reaction (PCR; Phusion Hot Start II DNA polymerase, catalog no. F549, Thermo Fisher Scientific) to amplify the targeted region. The resulting PCR products were screened for loss of the AflII restriction site for Tsc1, and SphI restriction site for Tsc2. PCR products of restriction site mutants were purified (GeneJet PCR Purification Kit, Thermo Fisher Scientific) and sequenced (CCHMC DNA Sequencing and Genotyping Core). For each gene, we selected clones that had, in both alleles, a frame-shifting mutation that resulted in an early stop codon.

Clonality assay

A modified clonality assay was used as previously described (PMID: 15104360). DNA was extracted from cortical tissues of wild-type and cyst walls of 11-week *Aqp2CreTsc2* female-mice using commercial kit (PureLink, Thermo Fisher Scientific, USA). Total of 50ng of DNA were digested first with 1.7U of BfaI for 1-hr followed by heat inactivation. This was followed by digestion with either 2U of methyl-sensitive HpaII or 4U methyl-insensitive MspII as a control in total of 15ul reaction. Similar protocol followed for undigested sample in which no HpaII or MspI was added. Total of 2ul of undigested , HpaII and MspI digestion product were used to amplify the 7th CpG island of mouse X-linked *pgk-1* promoter with following primers: CGCTGTTCTCCTCTTCCTCA (forward) and GGACGCAGAAAA-GCAAACTC (reverse). PCR products were separated in 1% agarose gel.

Extracellular vesicle isolation

Cells were serum starved for twenty-fouor hours. Serum free media were replaced and harvested after twenty-fouor hour incubation. The conditioned media were centrifuged at 2000g, 4˚C for 30min to remove cells and debris. The supernatants were transfered to new tubes with a half volume of total Exosome Isolation reagent (Cat. # 4478359, Thermofisher Scientific). The tubes were mixed well and incubated overnight at 4°C, and c entrifuged at 10,000g for one hour

at 4 ˚C. The supernatant was aspirated and discarded, and the pelleted extracellular vesicles were resuspended in phosphate buffered saline.

Human Imaging Studies

Following IRB approval, sequential de-identified patient imaging was evalulated for cystic burden by cyst count.

Statistics

All statistical analyses were performed using the R package version 3.1.0 (92). Cox proportional hazard models were performed using the Survival package (version 2.38-3; (93, 94)). Animals that died due to sacrifice or disease-related death were censored from the analyses.

Acknowledgements:

This work was supported by DoD grant W81XWH-14-1-0343(JJB), NIH grant DK107535, Le Bonheur Grant 650700 and funds from the Memphis Research Consortium (DB), NIH Grant HL48459(KWG) and NIH R21 12121(KWG), Veterans Administration (5 I01 BX001000-06) and Center for Genetics of Transport and Epithelial Biology (MS). This work utilized core facilities supported by Roswell Park Cancer Institute and NIH grant P30CA016056. This work is also supported by the Agliata family in memory of Jacob.

References

1. **Armour EA, Carson RP, and Ess KC**. Cystogenesis and elongated primary cilia in Tsc1-deficient distal convoluted tubules. *Am J Physiol Renal Physiol* 303: F584-592, 2012.

2. **Arulrajah S, Ertan G, Jordan L, Tekes A, Khaykin E, Izbudak I, and Huisman TA**. Magnetic resonance imaging and diffusion-weighted imaging of normal-appearing white matter in children and young adults with tuberous sclerosis complex. *Neuroradiology* 51: 781-786, 2009.

3. **Badenas C, Torra R, Perez-Oller L, Mallolas J, Talbot-Wright R, Torregrosa V, and Darnell A**. Loss of heterozygosity in renal and hepatic epithelial cystic cells from ADPKD1 patients. *Eur J Hum Genet* 8: 487-492, 2000.

4. **Barone S, Xu J, Zahedi K, Brooks M, and Soleimani M**. Probenecid Pre-treatment Downregulates the Kidney Cl(-)/HCO3(-) Exchanger (Pendrin) and Potentiates Hydrochlorothiazide-Induced Diuresis. *Front Physiol* 9: 849, 2018.

5. **Benvenuto G, Li S, Brown SJ, Braverman R, Vass WC, Cheadle JP, Halley DJ, Sampson JR, Wienecke R, and DeClue JE**. The tuberous sclerosis-1 (TSC1) gene product hamartin suppresses cell growth and augments the expression of the TSC2 product tuberin by inhibiting its ubiquitination. *Oncogene* 19: 6306-6316, 2000.

6. **Bissler JJ**. Cystic Kidney Diseases Associated with Increased Cancer Risk: Tuberous Sclerosis Complex, Von Hippel Lindau, and Birt Hogg Dubé. In: *Polycystic Kidney Disease: Translating Mechanisms into Therapy*, edited by Cowley BD, Jr., and Bissler JJ. New York: Springer, 2018, p. 51-66.

7. **Bissler JJ, and Kingswood C**. Renal Manifestation of Tuberous Sclerosis Complex. *Amer J Med Genet* Accepted: 2018.

8. **Bissler JJ, and Kingswood JC**. Optimal treatment of tuberous sclerosis complex associated renal angiomyolipomata: a systematic review. *Ther Adv Urol* 8: 279-290, 2016.

9. **Bissler JJ, Kingswood JC, Radzikowska E, Zonnenberg BA, Frost M, Belousova E, Sauter M, Nonomura N, Brakemeier S, de Vries PJ, Whittemore VH, Chen D, Sahmoud T, Shah G, Lincy J, Lebwohl D, and Budde K**. Everolimus for angiomyolipoma associated with tuberous sclerosis complex or sporadic lymphangioleiomyomatosis (EXIST-2): a multicentre, randomised, double-blind, placebo-controlled trial. *Lancet* 381: 817-824, 2013.

10. **Bissler JJ, McCormack FX, Young LR, Elwing JM, Chuck G, Leonard JM, Schmithorst VJ, Laor T, Brody AS, Bean J, Salisbury S, and Franz DN**. Sirolimus for angiomyolipoma in tuberous sclerosis complex or lymphangioleiomyomatosis. *N Engl J Med* 358: 140-151, 2008.

11. **Blake-Palmer KG, and Karet FE**. Cellular physiology of the renal H+ATPase. *Curr Opin Nephrol Hypertens* 18: 433-438, 2009.

12. **Bongaarts A, Giannikou K, Reinten RJ, Anink JJ, Mills JD, Jansen FE, Spliet GMW, den Dunnen WFA, Coras R, Blumcke I, Paulus W, Scholl T, Feucht M, Kotulska K, Jozwiak S, Buccoliero AM, Caporalini C, Giordano F, Genitori L, Soylemezoglu F, Pimentel J, Nellist M, Schouten-van Meeteren AYN, Nag A, Muhlebner A, Kwiatkowski DJ, and Aronica E**. Subependymal giant cell astrocytomas in Tuberous Sclerosis Complex have

consistent TSC1/TSC2 biallelic inactivation, and no BRAF mutations. *Oncotarget* 8: 95516-95529, 2017.

13. **Bonsib SM, Boils C, Gokden N, Grignon D, Gu X, Higgins JP, Leroy X, McKenney JK, Nasr SH, Phillips C, Sangoi AR, Wilson J, and Zhang PL**. Tuberous sclerosis complex: Hamartin and tuberin expression in renal cysts and its discordant expression in renal neoplasms. *Pathol Res Pract* 212: 972-979, 2016.

14. **Brasier JL, and Henske EP**. Loss of the polycystic kidney disease (PKD1) region of chromosome 16p13 in renal cyst cells supports a loss-of-function model for cyst pathogenesis. *Journal of Clinical Investigation* 99: 194-199, 1997.

15. **Breton S, and Brown D**. Regulation of luminal acidification by the V-ATPase. *Physiology (Bethesda)* 28: 318-329, 2013.

16. **Brook-Carter PT, Peral B, Ward CJ, Thompson P, Hughes J, Maheshwar MM, Nellist M, Gamble V, Harris PC, and Sampson JR**. Deletion of the TSC2 and PKD1 genes associated with severe infantile polycystic kidney disease--a contiguous gene syndrome. *Nat Genet* 8: 328-332, 1994.

17. **Brown D, Paunescu TG, Breton S, and Marshansky V**. Regulation of the V-ATPase in kidney epithelial cells: dual role in acid-base homeostasis and vesicle trafficking. *J Exp Biol* 212: 1762-1772, 2009.

18. **Cai S, Everitt JI, Kugo H, Cook J, Kleymenova E, and Walker CL**. Polycystic kidney disease as a result of loss of the tuberous sclerosis 2 tumor suppressor gene during development. *Am J Pathol* 162: 457-468, 2003.

19. **Cao T, and Feng Y**. The (pro)renin receptor and body fluid homeostasis. *Am J Physiol Regul Integr Comp Physiol* 305: R104-106, 2013.

20. **Cell_Signaling_Technology**. https://www.cellsignal.com/products/primary-antibodies/tuberin-tsc2-antibody/3612. 2018].

21. **Chen Z, Dong H, Jia C, Song Q, Chen J, Zhang Y, Lai P, Fan X, Zhou X, Liu M, Lin J, Yang C, Li M, Gao T, and Bai X**. Activation of mTORC1 in collecting ducts causes hyperkalemia. *J Am Soc Nephrol* 25: 534-545, 2014.

22. **Crambert G**. H-K-ATPase type 2: relevance for renal physiology and beyond. *Am J Physiol Renal Physiol* 306: F693-700, 2014.

23. **Crino PB, Aronica E, Baltuch G, and Nathanson KL**. Biallelic TSC gene inactivation in tuberous sclerosis complex. *Neurology* 74: 1716-1723, 2010.

24. **Dabora SL, Jozwiak S, Franz DN, Roberts PS, Nieto A, Chung J, Choy YS, Reeve MP, Thiele E, Egelhoff JC, Kasprzyk-Obara J, Domanska-Pakiela D, and Kwiatkowski DJ**. Mutational analysis in a cohort of 224 tuberous sclerosis patients indicates increased severity of TSC2, compared with TSC1, disease in multiple organs. *Am J Hum Genet* 68: 64-80, 2001.

25. **Danser AH**. The Role of the (Pro)renin Receptor in Hypertensive Disease. *American journal of hypertension* 28: 1187-1196, 2015.

26. **de Lemos Barbosa CM, Souza-Menezes J, Amaral AG, Onuchic LF, Cebotaru L, Guggino WB, and Morales MM**. Regulation of CFTR Expression and Arginine Vasopressin Activity Are Dependent on Polycystin-1 in Kidney-Derived Cells. *Cellular physiology and biochemistry : international journal of experimental cellular physiology, biochemistry, and pharmacology* 38: 28-39, 2016.

27. **Dodd KM, Yang J, Shen MH, Sampson JR, and Tee AR**. mTORC1 drives HIF-1alpha and VEGF-A signalling via multiple mechanisms involving 4E-BP1, S6K1 and STAT3. *Oncogene* 34: 2239-2250, 2015.

28. **Doench JG, Fusi N, Sullender M, Hegde M, Vaimberg EW, Donovan KF, Smith I, Tothova Z, Wilen C, Orchard R, Virgin HW, Listgarten J, and Root DE**. Optimized sgRNA design to maximize activity and minimize off-target effects of CRISPR-Cas9. *Nat Biotechnol* 34: 184-191, 2016.

29. **Doench JG, Hartenian E, Graham DB, Tothova Z, Hegde M, Smith I, Sullender M, Ebert BL, Xavier RJ, and Root DE**. Rational design of highly active sgRNAs for CRISPR-Cas9-mediated gene inactivation. *Nat Biotechnol* 32: 1262-1267, 2014.

30. **Dziedzic K, Pleniceanu O, and Dekel B**. Kidney stem cells in development, regeneration and cancer. *Semin Cell Dev Biol* 36: 57-65, 2014.

31. **Elorza A, Soro-Arnaiz I, Melendez-Rodriguez F, Rodriguez-Vaello V, Marsboom G, de Carcer G, Acosta-Iborra B, Albacete-Albacete L, Ordonez A, Serrano-Oviedo L, Gimenez-Bachs JM, Vara-Vega A, Salinas A, Sanchez-Prieto R, Martin del Rio R, Sanchez-Madrid F, Malumbres M, Landazuri MO, and Aragones J**. HIF2alpha acts as an mTORC1 activator through the amino acid carrier SLC7A5. *Mol Cell* 48: 681-691, 2012.

32. **Ertan G, Arulrajah S, Tekes A, Jordan L, and Huisman TA**. Cerebellar abnormality in children and young adults with tuberous sclerosis complex: MR and diffusion weighted imaging findings. *J Neuroradiol* 37: 231-238, 2010.

33. **Ewalt DH, Sheffield E, Sparagana SP, Delgado MR, and Roach ES**. Renal lesion growth in children with tuberous sclerosis complex. *J Urol* 160: 141-145, 1998.

34. **Fernandez R, Bosqueiro JR, Cassola AC, and Malnic G**. Role of Cl- in electrogenic H+ secretion by cortical distal tubule. *J Membr Biol* 157: 193-201, 1997.

35. **Franz DN**. Everolimus in the treatment of subependymal giant cell astrocytomas, angiomyolipomas, and pulmonary and skin lesions associated with tuberous sclerosis complex. *Biologics* 7: 211-221, 2013.

36. **Franz DN, Budde K, Kingswood JC, Belousova E, Sparagana S, de Vries PJ, Berkowitz N, Ridolfi A, and Bissler JJ**. Effect of everolimus on skin lesions in patients treated for subependymal giant cell astrocytoma and renal angiomyolipoma: final 4-year results from the randomised EXIST-1 and EXIST-2 studies. *J Eur Acad Dermatol Venereol* 2018.

37. **Gennari FJ**. Pathophysiology of metabolic alkalosis: a new classification based on the centrality of stimulated collecting duct ion transport. *Am J Kidney Dis* 58: 626-636, 2011.

38. **Glenn ST, Jones CA, Pan L, and Gross KW**. In vivo analysis of key elements within the renin regulatory region. *Physiol Genomics* 35: 243-253, 2008.

39. **Grantham JJ**. Rationale for early treatment of polycystic kidney disease. *Pediatr Nephrol* 30: 1053-1062, 2015.

40. **Grantham JJ, Geiser JL, and Evan AP**. Cyst formation and growth in autosomal dominant polycystic kidney disease. *Kidney International* 31: 1145-1152, 1987.

41. **Harris PC**. Molecular basis of polycystic kidney disease: PKD1, PKD2 and PKHD1. *Curr Opin Nephrol Hypertens* 11: 309-314, 2002.

42. **Hasumi Y, Baba M, Ajima R, Hasumi H, Valera VA, Klein ME, Haines DC, Merino MJ, Hong SB, Yamaguchi TP, Schmidt LS, and Linehan WM**. Homozygous loss of BHD causes early embryonic lethality and kidney tumor development with activation of mTORC1 and mTORC2. *Proc Natl Acad Sci U S A* 106: 18722-18727, 2009.

43. **Henske EP, Neumann HP, Scheithauer BW, Herbst EW, Short MP, and Kwiatkowski DJ**. Loss of heterozygosity in the tuberous sclerosis (TSC2) region of

chromosome band 16p13 occurs in sporadic as well as TSC-associated renal angiomyolipomas. *Genes Chromosomes Cancer* 13: 295-298, 1995.

44. **Henske EP, Scheithauer BW, Short MP, Wollmann R, Nahmias J, Hornigold N, van Slegtenhorst M, Welsh CT, and Kwiatkowski DJ**. Allelic loss is frequent in tuberous sclerosis kidney lesions but rare in brain lesions. *Am J Hum Genet* 59: 400-406, 1996.

45. **Hogan MC, Manganelli L, Woollard JR, Masyuk AI, Masyuk TV, Tammachote R, Huang BQ, Leontovich AA, Beito TG, Madden BJ, Charlesworth MC, Torres VE, LaRusso NF, Harris PC, and Ward CJ**. Characterization of PKD protein-positive exosome-like vesicles. *J Am Soc Nephrol* 20: 278-288, 2009.

46. **Hsu PD, Scott DA, Weinstein JA, Ran FA, Konermann S, Agarwala V, Li Y, Fine EJ, Wu X, Shalem O, Cradick TJ, Marraffini LA, Bao G, and Zhang F**. DNA targeting specificity of RNA-guided Cas9 nucleases. *Nat Biotechnol* 31: 827-832, 2013.

47. **Janicke M, Carney TJ, and Hammerschmidt M**. Foxi3 transcription factors and Notch signaling control the formation of skin ionocytes from epidermal precursors of the zebrafish embryo. *Dev Biol* 307: 258-271, 2007.

48. **Jones AC, Daniells CE, Snell RG, Tachataki M, Idziaszczyk SA, Krawczak M, Sampson JR, and Cheadle JP**. Molecular genetic and phenotypic analysis reveals differences between TSC1 and TSC2 associated familial and sporadic tuberous sclerosis. *Hum Mol Genet* 6: 2155-2161, 1997.

49. **Julian LM, and Stanford WL**. Reprogramming patient-derived tumor cells generates model cell lines for tuberous sclerosis-associated lymphangioleiomyomatosis. *Oncoscience* 4: 170-172, 2017.

50. **Jurkiewicz E, Jozwiak S, Bekiesinska-Figatowska M, and Walecki J**. Apparent diffusion coefficient is increased in children with tuberous sclerosis complex personal experience and review of the literature. *Neuroradiol J* 20: 622-626, 2007.

51. **Kanemoto S, Nitani R, Murakami T, Kaneko M, Asada R, Matsuhisa K, Saito A, and Imaizumi K**. Multivesicular body formation enhancement and exosome release during endoplasmic reticulum stress. *Biochem Biophys Res Commun* 480: 166-172, 2016.

52. **Kaneshiro Y, Ichihara A, Takemitsu T, Sakoda M, Suzuki F, Nakagawa T, Hayashi M, and Inagami T**. Increased expression of cyclooxygenase-2 in the renal cortex of human prorenin receptor gene-transgenic rats. *Kidney Int* 70: 641-646, 2006.

53. **Kim H, Xu H, Yao Q, Li W, Huang Q, Outeda P, Cebotaru V, Chiaravalli M, Boletta A, Piontek K, Germino GG, Weinman EJ, Watnick T, and Qian F**. Ciliary membrane proteins traffic through the Golgi via a Rabep1/GGA1/Arl3-dependent mechanism. *Nat Commun* 5: 5482, 2014.

54. **Kim J, and Kim E**. Rag GTPase in amino acid signaling. *Amino Acids* 48: 915-928, 2016.

55. **King HW, Michael MZ, and Gleadle JM**. Hypoxic enhancement of exosome release by breast cancer cells. *BMC cancer* 12: 421, 2012.

56. **Kwiatkowski DJ, Zhang H, Bandura JL, Heiberger KM, Glogauer M, el-Hashemite N, and Onda H**. A mouse model of TSC1 reveals sex-dependent lethality from liver hemangiomas, and up-regulation of p70S6 kinase activity in Tsc1 null cells. *Hum Mol Genet* 11: 525-534., 2002.

57. **Lam HC, Nijmeh J, and Henske EP**. New developments in the genetics and pathogenesis of tumours in tuberous sclerosis complex. *J Pathol* 241: 219-225, 2017.

58. **Lee BS**. Regulation of V-ATPase expression in mammalian cells. *Curr Protein Pept Sci* 13: 107-116, 2012.

59. **Maas SLN, Breakefield XO, and Weaver AM**. Extracellular Vesicles: Unique Intercellular Delivery Vehicles. *Trends Cell Biol* 27: 172-188, 2017.

60. **McCormack FX, Inoue Y, Moss J, Singer LG, Strange C, Nakata K, Barker AF, Chapman JT, Brantly ML, Stocks JM, Brown KK, Lynch JP, 3rd, Goldberg HJ, Young LR, Kinder BW, Downey GP, Sullivan EJ, Colby TV, McKay RT, Cohen MM, Korbee L, Taveira-DaSilva AM, Lee HS, Krischer JP, and Trapnell BC**. Efficacy and safety of sirolimus in lymphangioleiomyomatosis. *N Engl J Med* 364: 1595-1606, 2011.

61. **Onda H, Lueck A, Marks PW, Warren HB, and Kwiatkowski DJ**. Tsc2(+/-) mice develop tumors in multiple sites that express gelsolin and are influenced by genetic background. *J Clin Invest* 104: 687-695, 1999.

62. **Parolini I, Federici C, Raggi C, Lugini L, Palleschi S, De Milito A, Coscia C, Iessi E, Logozzi M, Molinari A, Colone M, Tatti M, Sargiacomo M, and Fais S**. Microenvironmental pH is a key factor for exosome traffic in tumor cells. *J Biol Chem* 284: 34211-34222, 2009.

63. **Parry L, Maynard JH, Patel A, Hodges AK, von Deimling A, Sampson JR, and Cheadle JP**. Molecular analysis of the TSC1 and TSC2 tumour suppressor genes in sporadic glial and glioneuronal tumours. *Hum Genet* 107: 350-356, 2000.

64. **Patel B, Patel J, Cho JH, Manne S, Bonala S, Henske E, Roegiers F, Markiewski M, and Karbowniczek M**. Exosomes mediate the acquisition of the disease phenotypes by cells with normal genome in tuberous sclerosis complex. *Oncogene* 35: 3027-3036, 2016.

65. **Pema M, Drusian L, Chiaravalli M, Castelli M, Yao Q, Ricciardi S, Somlo S, Qian F, Biffo S, and Boletta A**. mTORC1-mediated inhibition of polycystin-1 expression drives renal cyst formation in tuberous sclerosis complex. *Nat Commun* 7: 10786, 2016.

66. **Pena-Llopis S, and Brugarolas J**. TFEB, a novel mTORC1 effector implicated in lysosome biogenesis, endocytosis and autophagy. *Cell Cycle* 10: 3987-3988, 2011.

67. **Pena-Llopis S, Vega-Rubin-de-Celis S, Schwartz JC, Wolff NC, Tran TA, Zou L, Xie XJ, Corey DR, and Brugarolas J**. Regulation of TFEB and V-ATPases by mTORC1. *EMBO J* 30: 3242-3258, 2011.

68. **Peters J**. The (pro)renin receptor and its interaction partners. *Pflugers Arch* 469: 1245-1256, 2017.

69. **Pomatto MAC, Gai C, Bussolati B, and Camussi G**. Extracellular Vesicles in Renal Pathophysiology. *Front Mol Biosci* 4: 37, 2017.

70. **ProteinTech**. Tuberin-Specific Antibody Catalog number: 20004-1-AP https://www.ptglab.com/products/TSC2-Specific-Antibody-20004-1-AP.htm#validation. 2018].

71. **Quesenberry PJ, Aliotta J, Deregibus MC, and Camussi G**. Role of extracellular RNA-carrying vesicles in cell differentiation and reprogramming. *Stem Cell Res Ther* 6: 153, 2015.

72. **Rajagopal M, Thomas SV, Kathpalia PP, Chen Y, and Pao AC**. Prostaglandin E2 induces chloride secretion through crosstalk between cAMP and calcium signaling in mouse inner medullary collecting duct cells. *Am J Physiol Cell Physiol* 306: C263-278, 2014.

73. **Rakowski SK, Winterkorn EB, Paul E, Steele DJ, Halpern EF, and Thiele EA**. Renal manifestations of tuberous sclerosis complex: Incidence, prognosis, and predictive factors. *Kidney Int* 70: 1777-1782, 2006.

74. **Ramkumar N, and Kohan DE**. The nephron (pro)renin receptor: function and significance. *Am J Physiol Renal Physiol* 311: F1145-F1148, 2016.

75. **Ramkumar N, and Kohan DE**. Role of the Collecting Duct Renin Angiotensin System in Regulation of Blood Pressure and Renal Function. *Curr Hypertens Rep* 18: 29, 2016.

76. **Roux T, An-Gourfinkel I, Bertrand A, and Bielle F**. Astrocytic tumor with large cells and worrisome features in two patients with tuberous sclerosis: drastically different diagnoses and prognoses. *Clin Neuropathol* 36 (2017): 102-107, 2017.

77. **Roy A, Al-bataineh MM, and Pastor-Soler NM**. Collecting duct intercalated cell function and regulation. *Clinical journal of the American Society of Nephrology : CJASN* 10: 305-324, 2015.

78. **Saigusa T, Dang Y, Bunni MA, Amria MY, Steele SL, Fitzgibbon WR, and Bell PD**. Activation of the intrarenal renin-angiotensin-system in murine polycystic kidney disease. *Physiol Rep* 3: 2015.

79. **Sancak Y, Bar-Peled L, Zoncu R, Markhard AL, Nada S, and Sabatini DM**. Ragulator-Rag complex targets mTORC1 to the lysosomal surface and is necessary for its activation by amino acids. *Cell* 141: 290-303, 2010.

80. **Scheffers MS, van der Bent P, Prins F, Spruit L, Breuning MH, Litvinov SV, de Heer E, and Peters DJ**. Polycystin-1, the product of the polycystic kidney disease 1 gene, co-localizes with desmosomes in MDCK cells. *Hum Mol Genet* 9: 2743-2750, 2000.

81. **Seva Pessoa B, van der Lubbe N, Verdonk K, Roks AJ, Hoorn EJ, and Danser AH**. Key developments in renin-angiotensin-aldosterone system inhibition. *Nature reviews Nephrology* 9: 26-36, 2013.

82. **Sihn G, Burckle C, Rousselle A, Reimer T, and Bader M**. (Pro)renin receptor: subcellular localizations and functions. *Front Biosci (Elite Ed)* 5: 500-508, 2013.

83. **Siroky BJ, Czyzyk-Krzeska MF, and Bissler JJ**. Renal involvement in tuberous sclerosis complex and von Hippel-Lindau disease: shared disease mechanisms? *Nat Clin Pract Nephrol* 5: 143-156, 2009.

84. **Siroky BJ, Kleene NK, Kleene SJ, Varnell CD, Jr., Comer RG, Liu J, Lu L, Pachciarz NW, Bissler JJ, and Dixon BP**. Primary cilia regulate the osmotic stress response of renal epithelial cells through TRPM3. *Am J Physiol Renal Physiol* 312: F791-F805, 2017.

85. **Siroky BJ, Towbin AJ, Trout AT, Schafer H, Thamann AR, Agricola KD, Tudor C, Capal J, Dixon BP, Krueger DA, and Franz DN**. Improvement in Renal Cystic Disease of

Tuberous Sclerosis Complex After Treatment with Mammalian Target of Rapamycin Inhibitor. *J Pediatr* 187: 318-322 e312, 2017.

86. **Siroky BJ, Yin H, Babcock JT, Lu L, Hellmann AR, Dixon BP, Quilliam LA, and Bissler JJ**. Human TSC-associated renal angiomyolipoma cells are hypersensitive to ER stress. *Am J Physiol Renal Physiol* 303: F831-844, 2012.

87. **Siroky BJ, Yin H, Dixon BP, Reichert RJ, Hellmann AR, Ramkumar T, Tsuchihashi Z, Bunni M, Dillon J, Bell PD, Sampson JR, and Bissler JJ**. Evidence for pericyte origin of TSC-associated renal angiomyolipomas and implications for angiotensin receptor inhibition therapy. *Am J Physiol Renal Physiol* 307: F560-570, 2014.

88. **Snippert HJ, van der Flier LG, Sato T, van Es JH, van den Born M, Kroon-Veenboer C, Barker N, Klein AM, van Rheenen J, Simons BD, and Clevers H**. Intestinal crypt homeostasis results from neutral competition between symmetrically dividing Lgr5 stem cells. *Cell* 143: 134-144, 2010.

89. **Stillwell TJ, Gomez MR, and Kelalis PP**. Renal lesions in tuberous sclerosis. *J Urol* 138: 477-481, 1987.

90. **Stoos BA, Náray-Fejes-Tóth A, Carretero OA, Ito S, and Fejes-Tóth G**. Characterization of a mouse cortical collecting duct cell line. *Kidney International* 39: 1168-1175, 1991.

91. **Sullivan LP, Wallace DP, and Grantham JJ**. Epithelial transport in polycystic kidney disease. *Physiol Rev* 78: 1165-1191, 1998.

92. **Team RC**. R: A language and environment
for statistical computing R Foundation for Statistical Computing. http://www.R-project.org/.

93. **Therneau T**. A Package for Survival Analysis in S. version 2.38 https://CRAN.R-project.org/package=survival.

94. **Therneau TM, and Grambsch PM**. *Modeling Survival Data: Extending the Cox Model*. New York: Springer-Verlag, 2000, p. 350.

95. **Traykova-Brauch M, Schonig K, Greiner O, Miloud T, Jauch A, Bode M, Felsher DW, Glick AB, Kwiatkowski DJ, Bujard H, Horst J, von Knebel Doeberitz M, Niggli FK, Kriz W, Grone HJ, and Koesters R**. An efficient and versatile system for acute and chronic modulation of renal tubular function in transgenic mice. *Nat Med* 14: 979-984, 2008.

96. **van Rooijen E, van de Hoek G, Logister I, Ajzenberg H, Knoers N, van Eeden F, Voest EE, Schulte-Merker S, and Giles RH**. The von Hippel-Lindau Gene Is Required to Maintain Renal Proximal Tubule and Glomerulus Integrity in Zebrafish Larvae. *Nephron* 138: 310-323, 2018.

97. **Varasteh Kia M, Barone S, McDonough AA, Zahedi K, Xu J, and Soleimani M**. Downregulation of the Cl-/HCO3-Exchanger Pendrin in Kidneys of Mice with Cystic Fibrosis: Role in the Pathogenesis of Metabolic Alkalosis. *Cellular physiology and biochemistry : international journal of experimental cellular physiology, biochemistry, and pharmacology* 45: 1551-1565, 2018.

98. **Wilson C, Bonnet C, Guy C, Idziaszczyk S, Colley J, Humphreys V, Maynard J, Sampson JR, and Cheadle JP**. Tsc1 haploinsufficiency without mammalian target of rapamycin activation is sufficient for renal cyst formation in Tsc1+/- mice. *Cancer Res* 66: 7934-7938, 2006.

99. **Xu J, Barone S, Li H, Holiday S, Zahedi K, and Soleimani M**. Slc26a11, a chloride transporter, localizes with the vacuolar H(+)-ATPase of A-intercalated cells of the kidney. *Kidney Int* 80: 926-937, 2011.

100. **Zahedi K, Barone S, Xu J, and Soleimani M**. Potentiation of the effect of thiazide derivatives by carbonic anhydrase inhibitors: molecular mechanisms and potential clinical implications. *PLoS One* 8: e79327, 2013.

101. **Zhou J, Brugarolas J, and Parada LF**. Loss of Tsc1, but not Pten, in renal tubular cells causes polycystic kidney disease by activating mTORC1. *Hum Mol Genet* 18: 4428-4441, 2009.

102. **Zomer A, Maynard C, Verweij FJ, Kamermans A, Schafer R, Beerling E, Schiffelers RM, de Wit E, Berenguer J, Ellenbroek SIJ, Wurdinger T, Pegtel DM, and van Rheenen J**. In Vivo imaging reveals extracellular vesicle-mediated phenocopying of metastatic behavior. *Cell* 161: 1046-1057, 2015.

103. **Zoncu R, Bar-Peled L, Efeyan A, Wang S, Sancak Y, and Sabatini DM**. mTORC1 senses lysosomal amino acids through an inside-out mechanism that requires the vacuolar H(+)-ATPase. *Science* 334: 678-683, 2011.

Figure Legends:

Figure 1. *Tsc* renal cystic disease. (A) *AqpCreTsc2* kidneys at 11 weeks with significant renal cystic disease. (B) Coronal sections of the kidney in figure A. (C) Mouse kidneys from *RenCreTsc1* mouse with unilateral cystic disease. These are on the same size scale as in A. (D) Coronal section of kidney in figure C.

Figure 2. Cystic epithelium express tuberin and have not undergone Cre mediated recombination. (A) Western blot of hamartin and tuberin expression in IMCD cells and derived hamartin- (T1G and T1H) and tuberin-knockdown cells (T2H ad T2J). Knock-down of hamartin is known to reduce tuberin expression (4). (B) Section of mutant kidney cortex and medulla. While the principal cells should express aquaporin-2 and not tuberin, other cells that do not express aquaporin-2 should maintain tuberin expression. Cystic epithelium was restricted to the cortex and continued to express tuberin (yellow arrows). At higher magnifications (63X) some aquaporin expressing cells were identified (white arrows). The medullary cells, believed to be medullary collecting ducts, robustly expressed aquaporin-2. (C) Cystic epithelium exhibits a PCR band that is the correct size for the non-recombined *lox*P2 site. (D) Sequencing these bands reveal that they contain the *lox*P2 site indicating that they did not undergo Cre mediated recombination.

Figure 3. The Tsc1 gene has not undergone recombination in the cystic epithelium of the *Ren1cCreTsc1* model. (A) Brightfield of *Ren-1c-CreTsc1* kidney arteriole, denoted by 'v', and cysts, denoted by 'c'. (B) Fluorescence of the same tissue in panel A demonstrating vascular pericyte derived fluorescence, while cysts are devoid of signal. (C) Brightfield of arteriole and cysts. (D) Fluorescence of tissue in C with only vessel fluorescing.

Figure 4. Cyst epithelial phenotypes in *AqpCreTsc2* mice. (A) DBA staining in cyst epithelia in *AqpCreTsc2 (*Tsc-2 KO) mice. (B) Expression of AQP-2 in kidneys of WT (left) and *AqpCreTsc2 (*Tsc-2 KO) mice (right). (C) Double immunofluorescence labeling with AQP-2 (green) and H^+-ATPase (red) antibodies in normal kidney (merged image). (D) Double immunofluorescent labeling with AQP-2 (green) and H^+-ATPase (red) in kidneys of 5 weeks (left panel) and 11 weeks old (right panel) *AqpCreTsc2* mice (merged image). (E) Expression of prorenin receptor (PRR) in kidneys of *AqpCreTsc2* mouse. Left panel: normal kidney; Middle panel: 5 weeks old *AqpCreTsc2* mice. Right panel: 11 weeks old *AqpCreTsc2* mice. (F) Double

immunofluorescent labeling with NBC-e1 (right panel) and H^+-ATPase B subunit (left panel) in kidneys of 11 weeks old *AqpCreTsc2* mice. (G) Cyst double labeling with H^+-ATPase (green arrow) and AE-1 (red arrow), additional evidence that cystic epithelium consists of type A intercalated cells. (H) Double immunofluorescence labeling with H^+-ATPase and AQP-2 in kidneys of *Pkd1* mouse (merged image). (I) PCR products of female mouse *pgk*-1 promoter region on the X chromosome, for undigested sample, U, methyl-dependent *Hpa*II digested, H, and methyl-independent *Msp*I digested samples from WT and *AqpCreTsc2* mice. Cystic cell DNA is not clonal as band intensity is diminished by > 25% when input DNA is pre-digested with *Hpa*II. C: cyst, G: Glomerulus

Figure 5. *AqpCreTsc2* cystic epithelium exhibit much fewer primary cilia than adjacent tubules. (A) Immunofluorescence of acetylated tubulin (yellow arrow) easily identify primary cilia in a medullary collecting duct. (B-D) Cystic epithelium exhibit a significant suppression of primary cilia (white arrow) but does exhibit occasional cilia (yellow arrow).

Figure 6. Cyst epithelial phenotypes in *Ren1cCreTsc1* mice. (A) DBA staining in cyst epithelia in *Ren-1c- CreTsc1* (Tsc-1 KO) mice. (B) Expression of AQP-2 in kidneys of WT and *Ren1cCreTsc1* mice. (C) Double immunofluorescence labeling (merged image) with H^+-ATPase (green) and NBC-e1 (red) antibodies in normal kidney (left) and adult *Ren1cCreTsc1* mice (right). (D) Expression of PRR in kidneys of *Ren1cCreTsc1* mice. (E) Double immunofluorescence labeling with Na^+-K^+ ATPase (green) and NBC-e1 (red) in normal kidney (first and third panels) and *Ren1cCreTsc* mice (second and fourth panels). (F) Double immunofluorescence labeling with H^+-ATPase (red) and PCNA (Proliferating Cell Nuclear Antigen) antibodies (merged image) in kidneys WT, AqpCreTsc2, *RenCreTsc1* and *Pkd1* mice.

Figure 7. mTORC1 involved in cystic disease. (A) *AqpCreTsc2* cysts stain robustly for phospho-S6 (bar is 50 µm). (B) *RenCreTsc1* cysts also stain robustly for phospho-S6 (bar is 1000 µm). (C) mTORC1 inhibition significantly prolongs *AqpCreTsc2* survival compared to sham treated ($p=0.0293$) (n=5 mice each group). (D) mTORC1 inhibition also significantly prolongs *RenCreTsc1* survival compared to sham treated animals ($p<0.0001$) (n=10 mice each group).

Figure 8. Human Polycystic variety of TSC renal Disease. (A) Human polycystic kidney variety of TSC renal disease at nephrectomy. (B) Cyst epithelium from kidney in panel A exhibiting apical staining with H^+-ATPase antibody (bar is 100 µm). (C) Biopsy specimen from patient with TSC-related microcystic disease exhibiting apical staining with H^+-ATPase antibody (bar is 100 µm). (D) MRI imaging (T2 fast spin echo with fat suppression) from patients with TSC cystic disease (white lesions in solitary left kidney) before mTORC1 inhibitor therapy, (E) Patient in panel 'D' after one year on drug. (F) Analysis of total kidney cyst count from 5 patients with cortical cystic disease and focal cystic disease before and after mTORC1 therapy.

Figure 9. Inner medullary collecting duct (principal) cells produce extracellular vesicle that induce intercalated cell mTORC1 signaling. (A) Microscopic cyst containing extracellular vesicles in lumen (arrow). (B) Extracellular vesicles either budding from or fusing with apical epithelial cell surface (arrow). (C) Diagram of experimental design. Intercalated cells were exposed to principal cell derived conditioned media or isolated extracellular vesicles. (D) Western blot of phospho-S6 and S6 in cultured intercalated cells. To calibrate experiment, intercalated cells were exposed to FBS or serum starvation (FBS-), or isolated extracellular vesicles from 1 ml (ECV-1) or 3 ml (EVC-3) of the corresponding conditioned media. ** Student t test P-value <0.01.IMCD cells, derived hamartin- (T1G and T1H) and tuberin-knockdown cells (T2H ad T2J). Bar diagram shows optical density of three independent experiments (Mean ± SEM).

Figure 10. Model of TSC Cystogenesis. Cortical collecting duct contains three types of intercalated cells (see color key) and principal cells that express cilia (blue). Stimulation initiated from either the mutant principal cells or the mutant vascular pericytes (arrows), drive the type A intercalated cells to adopt a mutant phenotype and proliferate (dashed arrows).

Table 1: List of antibodies used in the study.

Antibody	Dilution	Source	Catalog Number

Alexa Fluor Donkey anti-Goat IgG	1:200	Invitrogen; Eugene, OR	A-11055
Alexa Fluor Goat anti-Mouse IgG	1:200	Invitrogen; Eugene, OR	A-11001
Alexa Fluor Goat anti-rabbit IgG	1:200	Invitrogen; Eugene, OR	A-11008
Anti-Hamartin	1:1,000	Cell Signaling Technology, Inc. Danvers, MA	4906
	1:1,000	ProteinTech Rabbit Polyclonal	209988-I-AP
Anti-Na^+/K^+ATPase		Dr. Jerry Lingrel, University of Cincinnati	
Anti-phospho-P70S6Kinase (Thr389)	1:5,000	Cell Signaling Technology, Inc. Danvers, MA	9205
Anti-Tuberin	1:2,000	Cell Signaling Technology, Inc. Danvers, MA	3612
Anti-Tuberin		ProteinTech Rabbit Polyclonal	20004-1-AP
Biotinylated Dolichos biflorus agglutinin (DBA)	1:300	Vector Laboratories, Burlingame, CA, USA	RL-1032
Biotinylated Lotus Tetragonolobus Lection (LTL)	1:2,000	Vector Laboratories, Burlingame, CA, USA	B-1325-2
Goat polyclonal Anti-PRR	1:50	Origene Technologies; Rockville, MD	
HMB-45	1:40	Thermo Scientific,Waltham, MA	MA5-16712
Mouse monoclonal Anti-AQP2	1:5,000	Dr. A. Blanchard, Paris-Descartes University	
Mouse monoclonal Anti-H+ATPase	1:25	Dr. S. Holliday, University of Florida	
Mouse monoclonal Anti-PCNA	1:100	Santa Cruz Biotechnologies; Dallas, TX	SC-56
Phospho-S6 Ribossoma Protein	1:5,000	Cell Signaling Technology, Inc. Danvers, MA	2211
Rabbit polyclonal Anti-H^+ATPase	1:100	Dr. M. Soleimani, University of Cincinnati	
Rabbit polyclonal Anti-NBCe1	1:40	Dr. M. Soleimani, University of Cincinnati	
Rabbit polyclonal Anti-NCC	1:60	Stressmarq Biosciences; Victoria, BC, Canada	SPC-402

Rabbit polyclonal Anti-NHE3	1:60	Dr. Alicia McDonough, University of California at Los Angeles	
Rabbit polyclonal Anti-Pendrin	1:15	Generated by Soleimani	
S100	1:100	Abcam, Cambridge, MA	ab52642

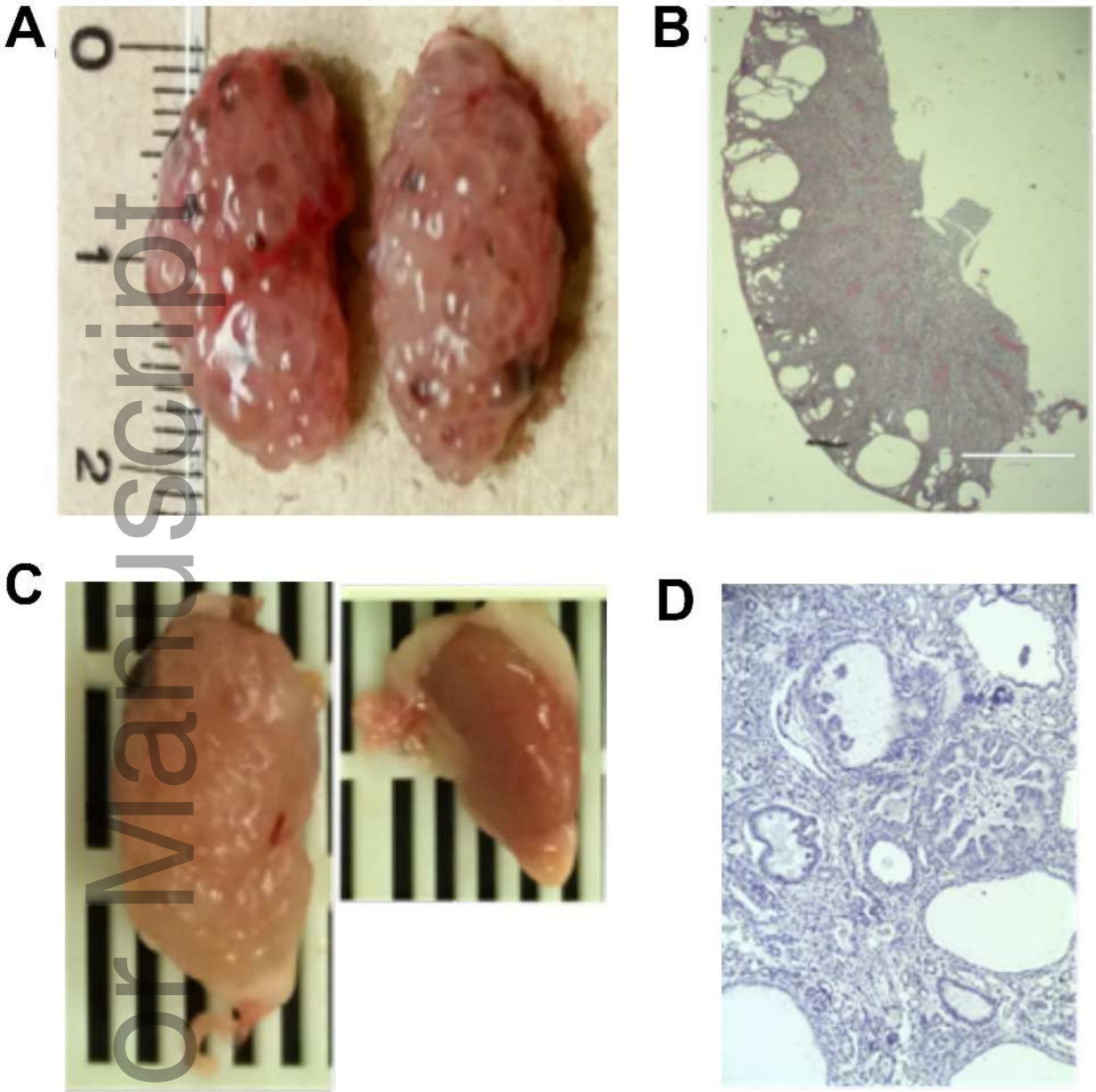

phy2_13983_f1.tiff

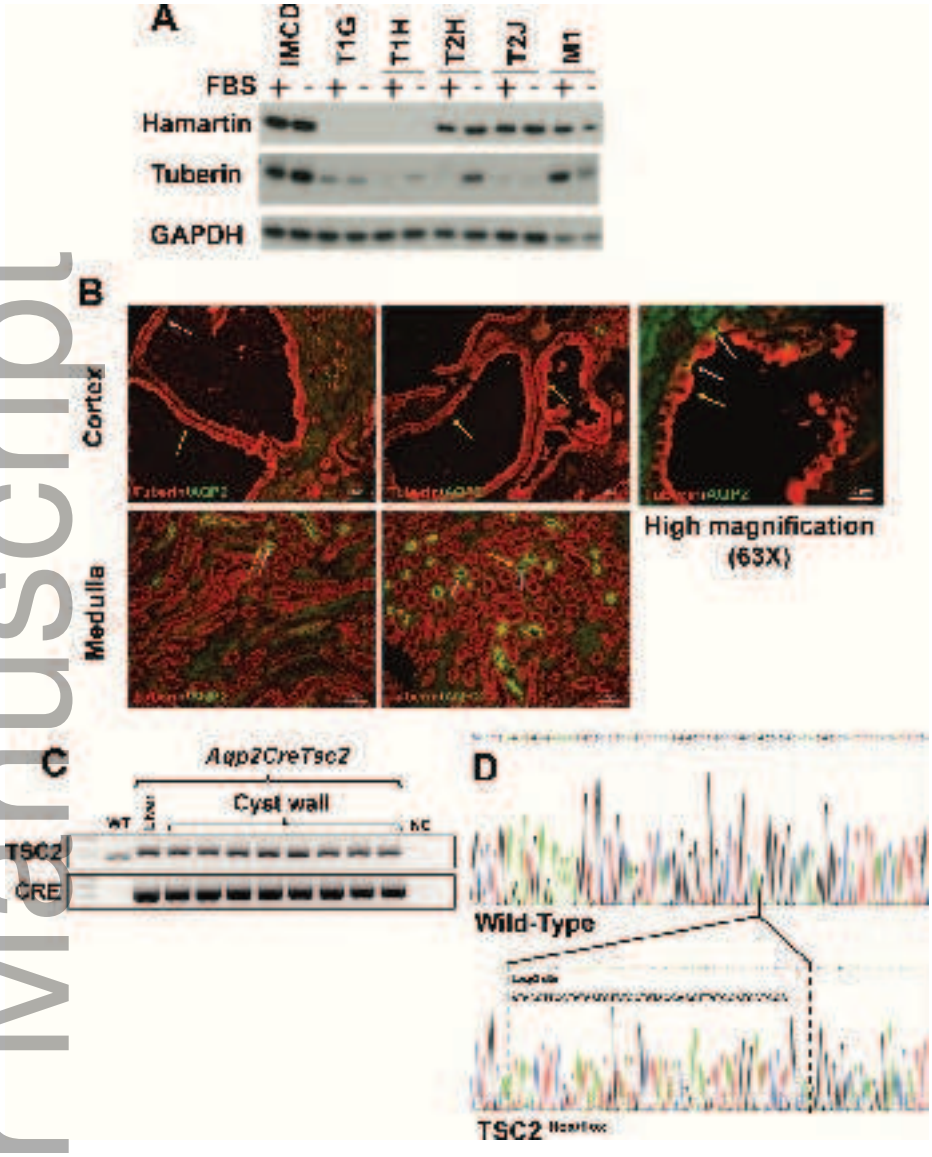

phy2_13983_f2.tif

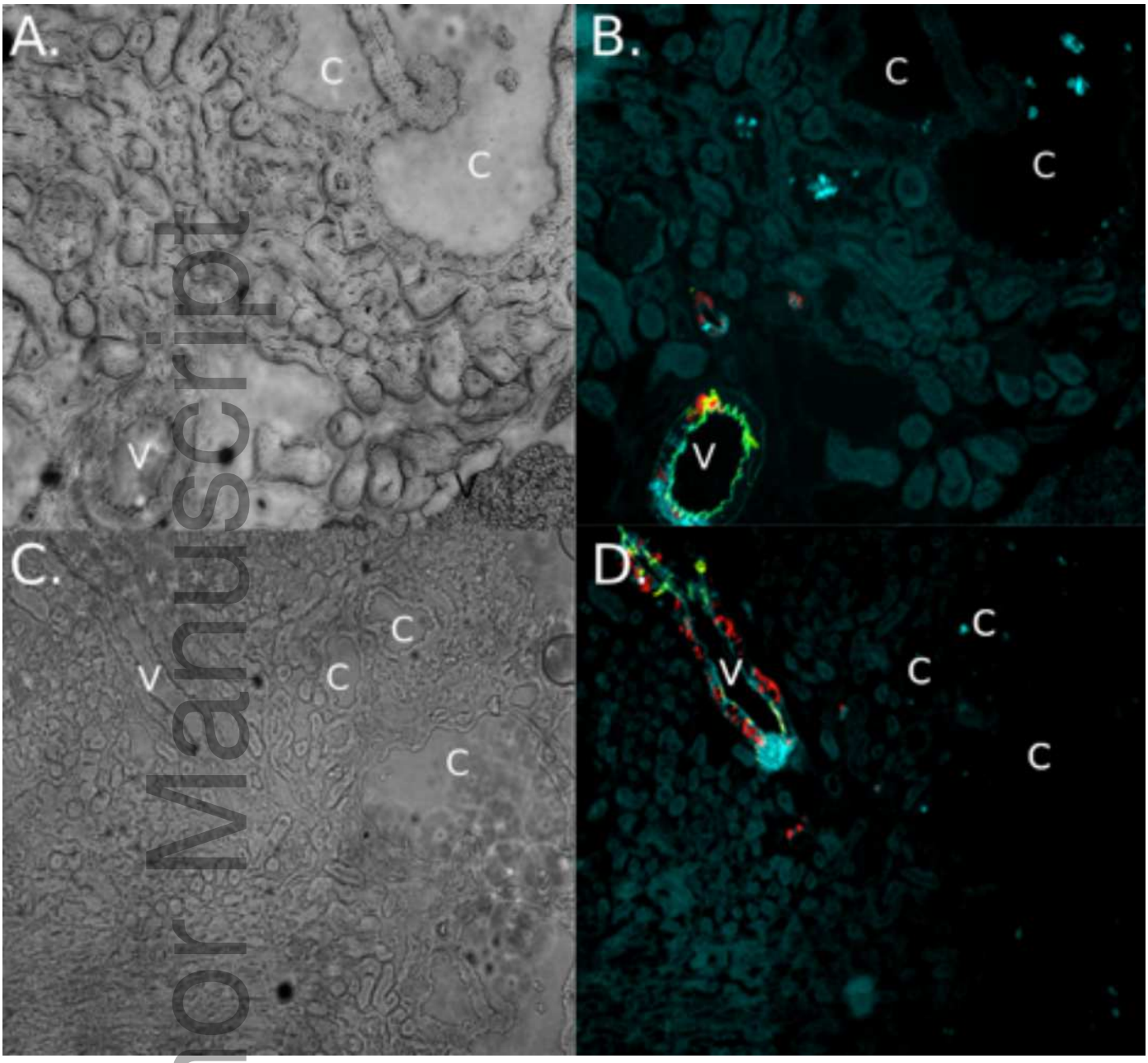

phy2_13983_f3.tif

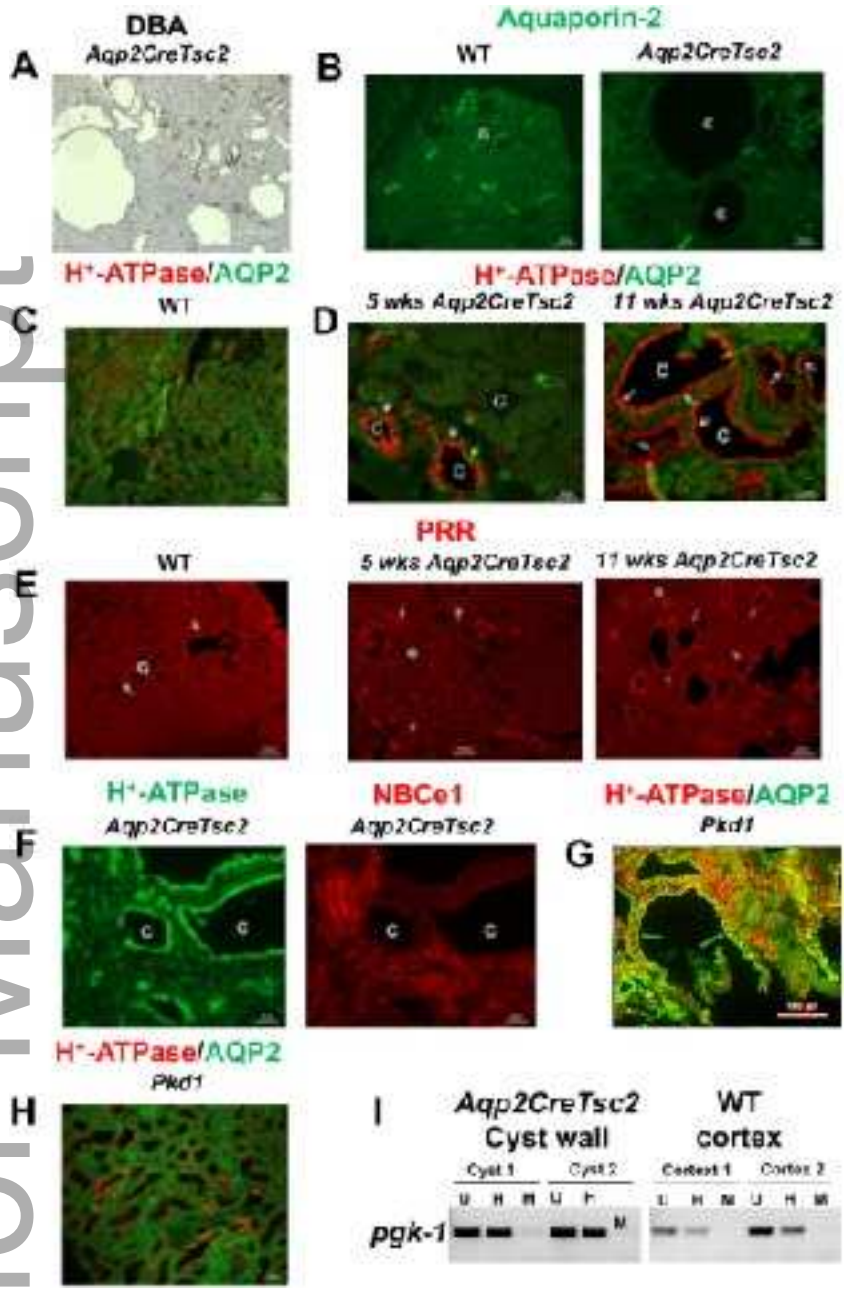

phy2_13983_f4.png

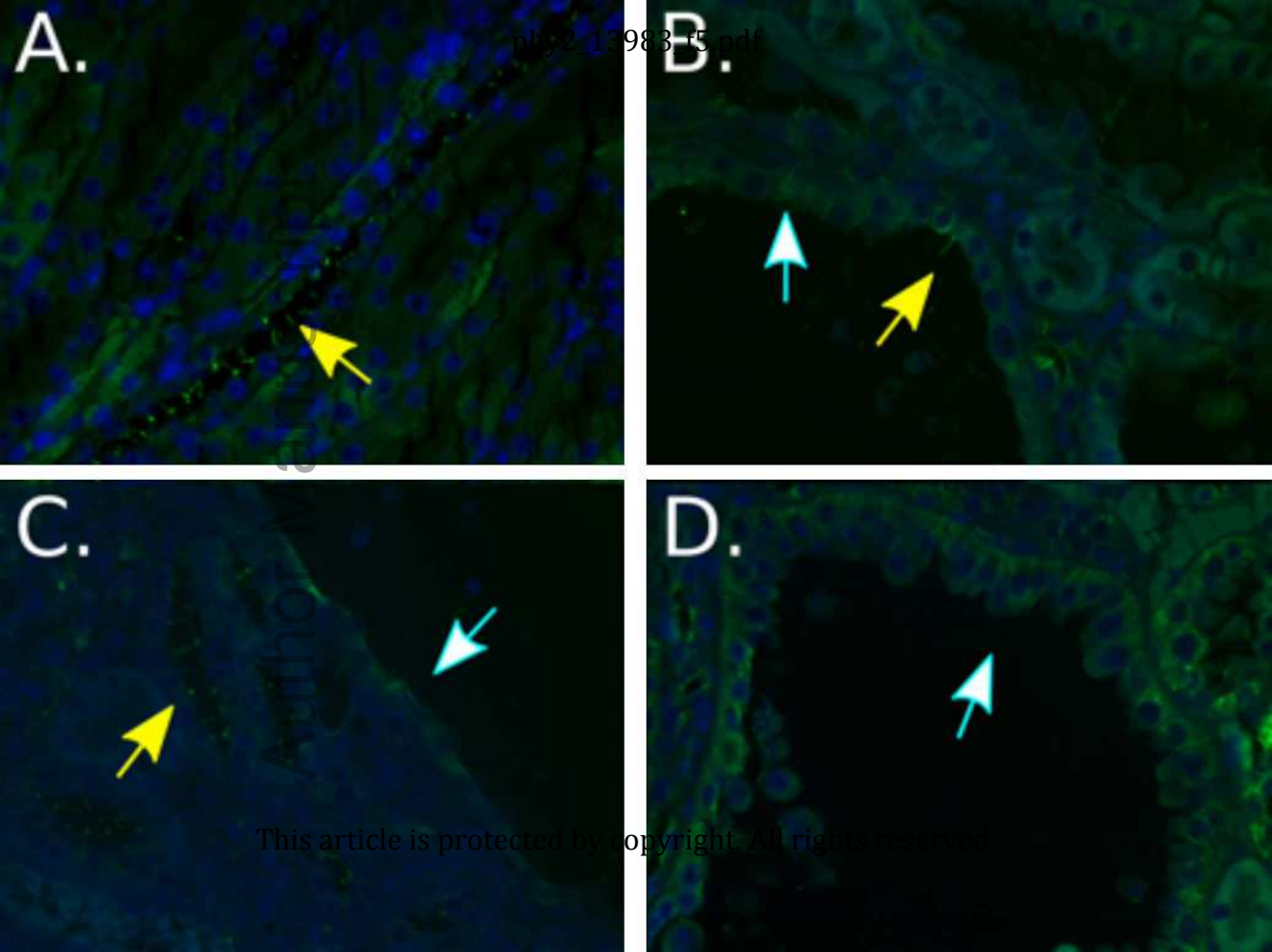

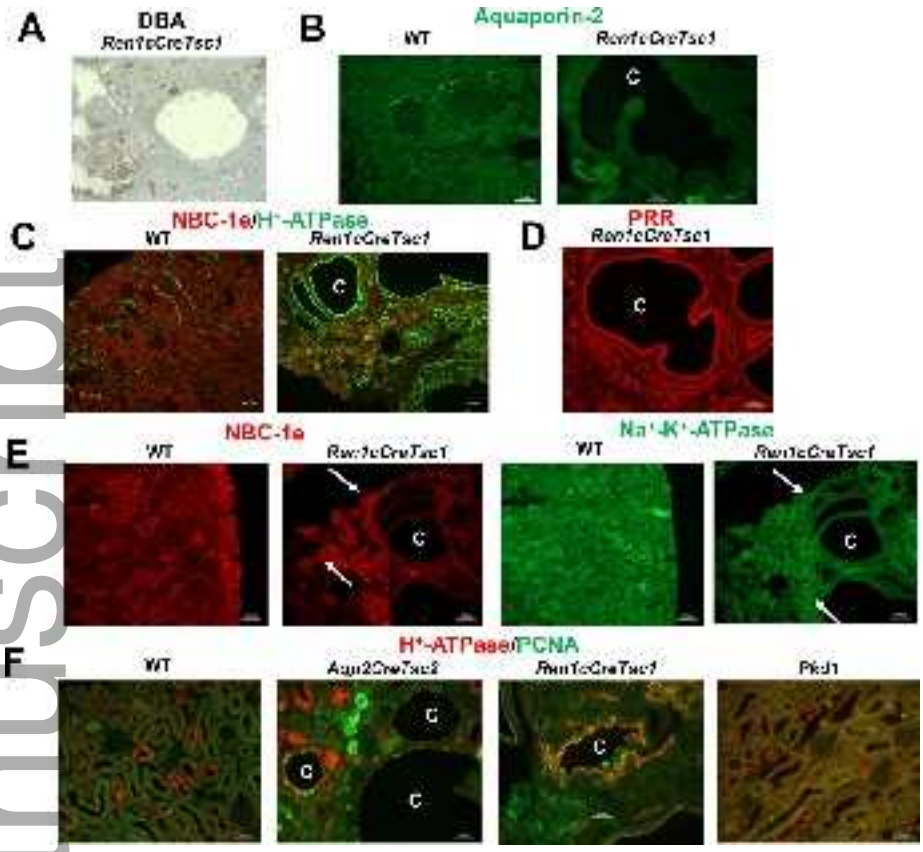

phy2_13983_f6.tif

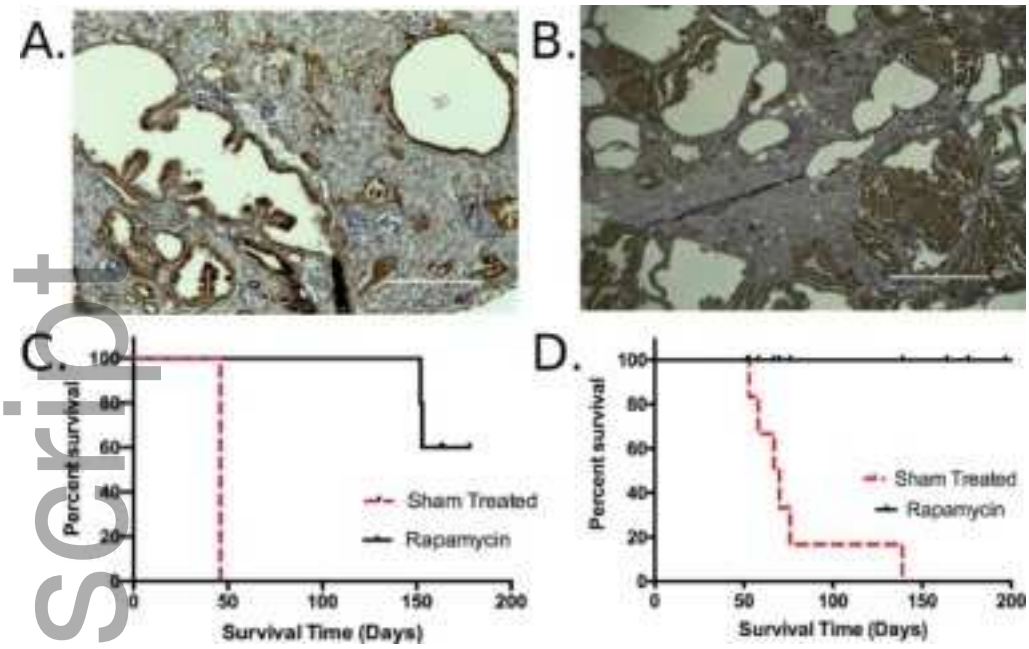

phy2_13983_f7.png

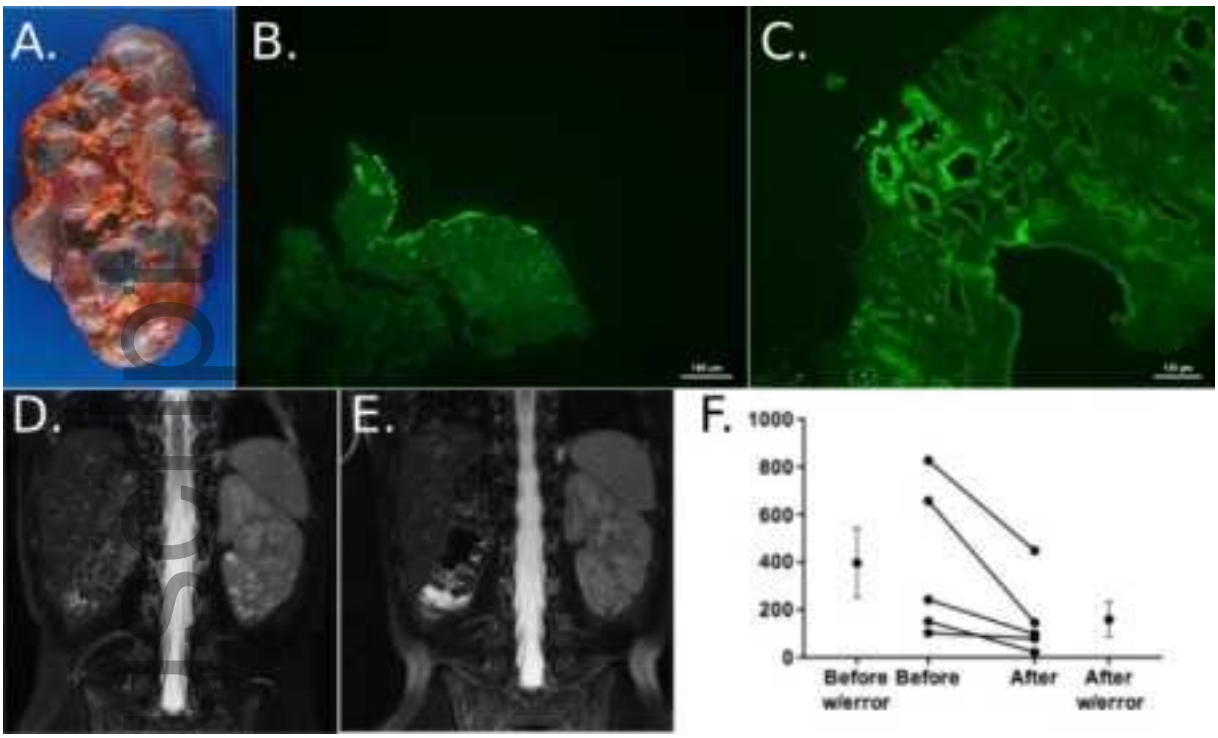

phy2_13983_f8.png

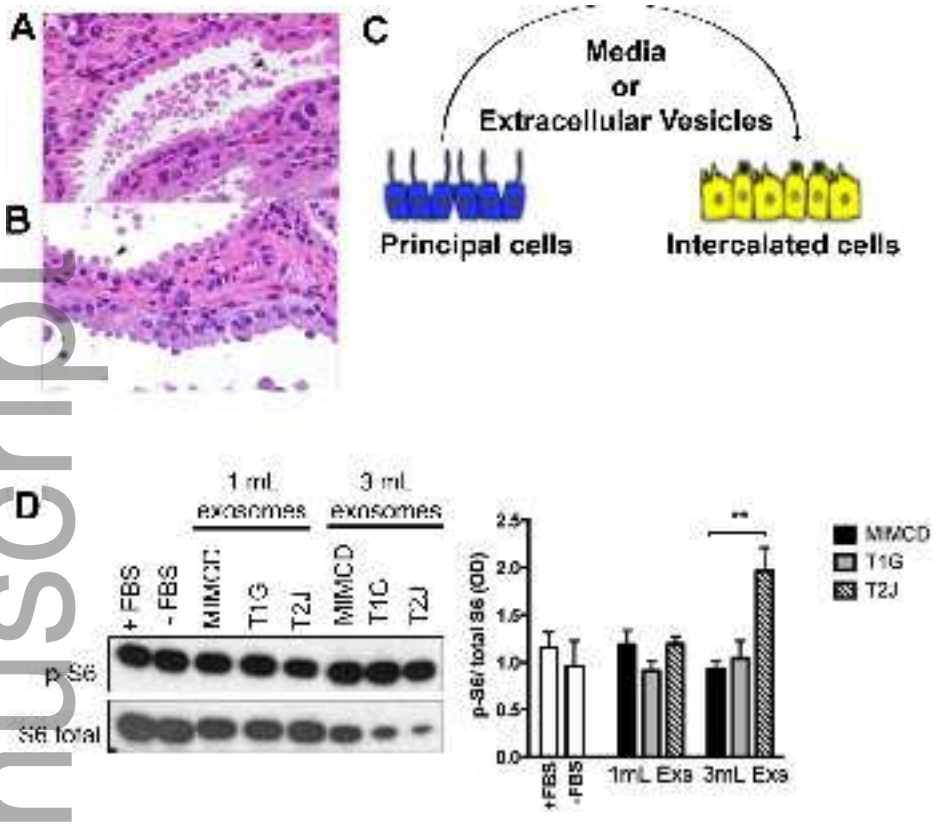

phy2_13983_f9.tif

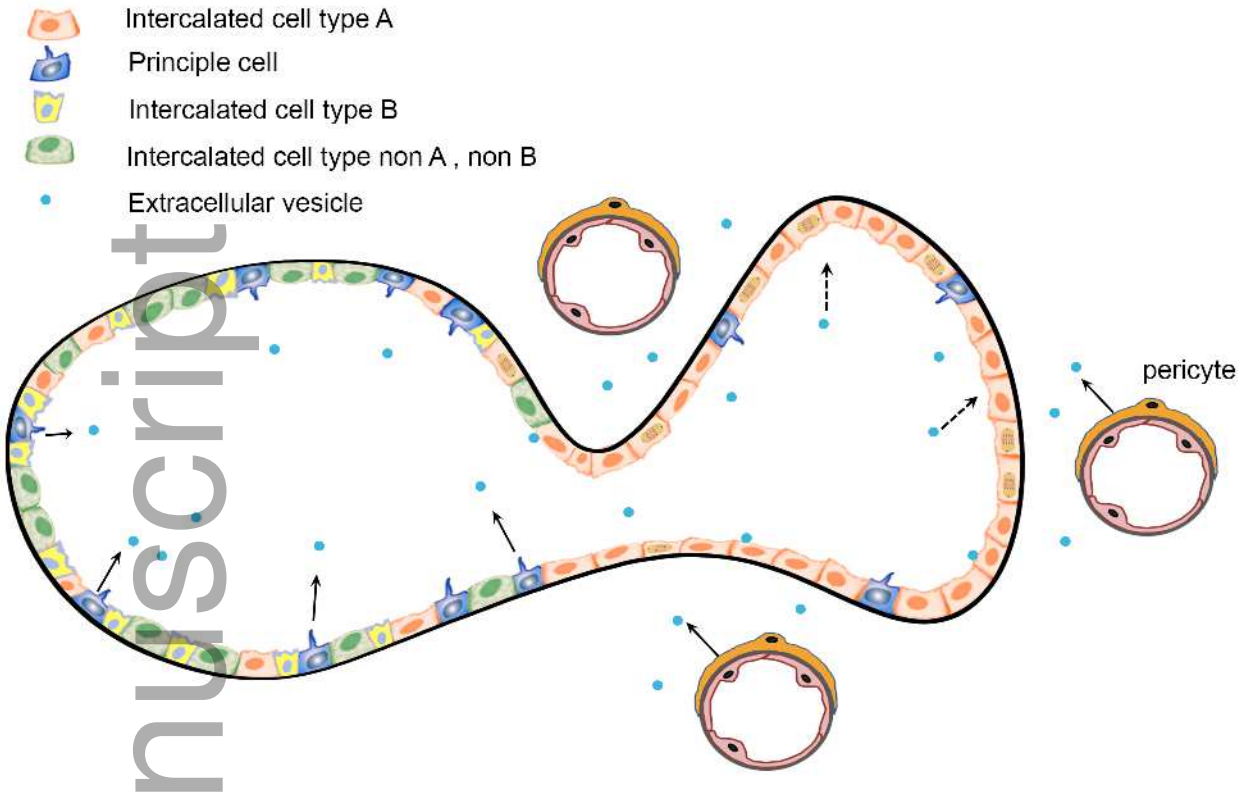

phy2_13983_f10.tif